CZECH TECHNICAL UNIVERSITY IN PRAGUE
FACULTY OF MECHANICAL ENGINEERING
DEPARTMENT OF ENVIRONMENTAL ENGINEERING

CFD MODEL AND SIMULATION FOR THE DESIGN OF A SPRAY BOOTH

DIPLOMA THESIS

NALUGOTLA ELIJAH MIGHT 1-EE-2018

MASTER'S THESIS ASSIGNMENT

I. Personal and study details

Student's name: **Nalugotla Elijah Might** Personal ID number: **465258**

Faculty / Institute: **Faculty of Mechanical Engineering**

Department / Institute: **Department of Environmental Engineering**

Study program: **Mechanical Engineering**

Branch of study: **Environmental Engineering**

II. Master's thesis details

Master's thesis title in English:

CFD Model and Simulation for the Design of a Spray Booth

Master's thesis title in Czech:

CFD model a simulace pro návrh stříkacího boxu

Guidelines:

Create a CFD model to simulate air flow in a spray booth with working chamber volume approx. 1 m3. Perform CFD simulations to assess different options of the exhaust opening(s) design with respect to the uniformity of air flow in the working chamber and the effectiveness of transport of paint particles to the filtration system.

Bibliography / sources:

ANSYS. Ansys 19 Documentation. Ansys, Inc., 2018.
ASHRAE Handbook of HVAC Applications. Chapter 16 - Laboratories. ASHRAE, 2015.
RJA. Spray Booth Design and Maintenance for Pollution Prevention. Ron Joseph & Associates, Inc., 1991.
TALBERT R. Paint Technology Handbook. Chapter 8 - Spray Booths. CRC Press (Taylor & Francis Group), 2008.

Name and workplace of master's thesis supervisor:

Ing. Martin Barták, Ph.D., Department of Environmental Engineering, FME

Name and workplace of second master's thesis supervisor or consultant:

Date of master's thesis assignment: **26.04.2018** Deadline for master's thesis submission: **22.06.2018**

Assignment valid until: _____

Ing. Martin Barták, Ph.D.	doc. Ing. Vladimír Zmrhal, Ph.D.	prof. Ing. Michael Valášek, DrSc.
Supervisor's signature	Head of department's signature	Dean's signature

III. Assignment receipt

The student acknowledges that the master's thesis is an individual work. The student must produce his thesis without the assistance of others, with the exception of provided consultations. Within the master's thesis, the author must state the names of consultants and include a list of references.

25.-04-2018
Date of assignment receipt

Student's signature

I declare that this diploma thesis entitled "CFD Model and Simulation for the Design of a Spray Booth" is my own work performed under the supervision of Ing. Martin Barták, Ph.D. with the use of the literature presented at the end of my diploma thesis in the list of references.

In Prague 22.06.2018 Nalugotla Elijah Might

Abstract

Effective ventilation of the paint particles and volatile organic compounds without disturbing the air flow in the working space are the most important characteristics of a spray booth. Spray booth should not disturb the efficiency of the spray painting process while achieving this. Various surveys have reported that large percentage of workers suffer from eye and respiratory discomfort, headaches and feelings of lethargy because of volatile organic compounds (VOCs). In a small-scale painting process, therefore, efficient ventilation system is very important for human health as well. In this study, various exhaust outlet and inlet options for a spray booth of approximately one cubic meter volume have been analyzed. A commercial software ANSYS FLUENT has been employed for CFD simulations. The air flow pattern in the working chamber with inlet velocities 0.5 and 2.5 m/s was studied and the particles of sizes 5 and 50 microns were tracked. The results show that the out of six exhaust variants, two are the best ways to exhaust the paint particles without letting any particles escape into the ambience.

Abstrakt

Účinný odvod částic barev a těkavých látek větráním při homogenním proudění vzduchu v pracovní oblasti je nejdůležitější vlastností lakovacího boxu. Zároveň nesmí být narušen proces samotného lakování. Z různých výzkumů je známo, že vysoké procento pracovníků v této oblasti trpí podrážděním očí a dýchacího ústrojí, bolestmi hlavy a pocity otupělosti kvůli působení těkavých organických látek (VOC). Při lakovacím procesu prováděném v menším měřítku je proto účinný systém pro odvod škodlivin větráním velmi důležitý pro zdraví osob. Studie se zabývá různými variantami umístění odváděcích otvorů v malém lakovacím boxu o objemu cca 1 m^3. K tomu byl použity CFD simulace a komerční software ANSYS FLUENT. Bylo analyzováno proudění v pracovní části boxu při vstupní rychlosti proudění vzduchu 0,5 a 2,5 m/s a sledován pohyb částic o velikosti 5 a 50 mikronů. Výsledky ukazují, že z šesti uvažovaných možností jsou dvě nejvhodnější a tyto zajišťují odvod částic bez úniku do okolního prostředí.

Contents

List of Figures

List of Symbols

a - Distance between the centres of two holes [m]

b - Side of the squared hole [m]

C_f - Skin friction coefficient [-]

d - Diameter of the circular hole [m]

d_h - hydraulic diameter of the perforated plate [m]

d_n- Nozzle diameter [m]

g_i - Gravitational component in the ith direction [m/s^2]

k - Turbulence kinetic energy [m^2/s^2]

l - Length of the perforated plate [m]

$\dot{m}$ - Mass flow rate [kg/s]

p - Width of the perforated plate [m]

Pr_t - Turbulent Prandtl number for energy (0.85)

S_{open} - Surface area of the holes [m^2]

S_{gross} - Surface area without holes [m^2]

u - Velocity of air at the filter [m/s]

u_{avg} - Average velocity in front of the filter [m/s]

u_s - Maximum spraying velocity [m/s]

u_∞- Velocity in the inlet of the model [m/s]

u_τ- Friction velocity [m/s]

$\overline{u_i}$ - Mean velocity component in corresponding direction [m/s]

$\dot{V}$ - Volumetric flow rate [m^3/s]

$\dot{V_p}$ - Maximum paint flow rate [m^3/s]

w - Distance between the centres of two holes [m]

x - Distance along the wall of the section [m]

y^+- Dimensionless distance from the wall [-]

ΔP_{avg} - Average pressure loss of the filter [Pa]

ΔP_{loss} - Pressure loss [Pa]

ΔP_s - Spray pressure [kPa]

ε - Dissipation rate of kinetic energy [m^2/s^3]

μ_t - Turbulent viscosity [m^2/s]

ν - Kinematic viscosity [m^2/s]

ρ - Density of the fluid [kg/m^3]

τ_w- Wall shear stress [Pa]

Φ - instantaneous variable

$\overline{\Phi}$ - mean component

Φ'- fluctuation component

1. Introduction

In the world where the combination of efficiency of the technology and the safety of the technician is vital, the necessity for the optimization of every appliance that comes into the market has increased.

Painting has been in use for centuries whether used for decorative or protective purposes. Significant developments have been made in the painting process and the devices used for painting. One of the most used painting technologies is spray painting. It is a process where the atomised paint is sprayed onto the object that is being painted. This technique helps to achieve a uniform and aesthetic paint film which is hard to achieve with a traditional paint brush.

Although spray painting is efficient, it has its disadvantages. One of them is the overspray. It is quite obvious that when the paint is atomised into small particles and sprayed, there definitely will be a part of it sprayed away from the target. Overspray is the leftover from the atomisation process and is a major concern that has to be dealt with in the spray painting process. It has been reported that volatile organic compounds (VOCs) that are released during the spray painting affect human health and productivity in a significant way. A major percentage of respiratory illnesses and lung cancers may be caused by avoidable indoor air pollutants such as VOCs (Chang, et al., 2002). When this overspray is inevitable there has to be a device or a technology that helps to trap and ventilate these harmful particulates, which brings us to the spray booths.

Spray booths are available in various designs based on the objects being sprayed, as big as rooms to spray the automobiles and as small as a box of one cubic meter volume to spray hand held objects. Several types of research have been conducted to improve the efficiency of the spray booth ventilation and the flow inside the booths. The placement of the exhaust plays a very important role in dictating the uniformity of air flow in the working space of the spray booth.

This thesis deals with the design of the exhaust opening of a portable spray booth to achieve a uniform air flow in the working chamber. Various options for the placement of the exhaust outlet have been studied. The air flow pattern in the device has been investigated using CFD simulations. ANSYS Fluent 19 was used as the simulation software.

The idea for the design was obtained from a technical report by Zelenský & Švandová, (2018). A number of exhaust outlet and inlet variants were designed and investigated in ANSYS Fluent to obtain the most efficient way to exhaust the paint particles without disturbing the flow in the working space. The simulations incorporated turbulence modelling to study the air flow pattern and discrete phase modelling to study the particles flow.

2. Literature review

2.1 Spray booth

A spray booth is a ventilated enclosure around the spray application operation, with the help of which the escape of the over sprayed material including the vapours that are not deposited on the object being sprayed is directed to the exhaust system. It contains the over sprayed paint and controls the spray environment providing a clean and safe workspace for the operator and also renders a smooth air flow to enhance the paint transfer efficiency. The spray booth is included with an exhaust fan which creates a negative air pressure inside the booth. The exhaust air containing the overspray is directed to the filters where the paint particulates are filtered, and the solvent vapours are directed to the atmosphere or an abatement system (Talbert, 2008).

Spray booths can be classified as follows

1. Based on the method of collecting overspray
    a. Dry filter spray booths
    b. Water wash booths
2. Based on the direction of air flow
    a. Down draft
    b. Cross draft
    c. Semi-down draft

2.1.1 Methods of collecting overspray

Dry filter spray booths

Exhaust filtration is designed to capture paint solids before passing into the exhaust air stream and then allow the solvent vapours to pass through into the exhaust air stream. It is common that in many systems two layers of filters are used to provide the needed particulate arresting efficiency while keeping the overall cost as low as possible and reducing filter change. However, the exact filter arrangement is always related to the requirements of the process. It depends on the material being sprayed, application equipment transfer efficiency, and amount of overspray.

The first layer of filters is usually less expensive. It is a coarse filter and is designed to collect the bulk of overspray and is less efficient on the small particle sizes. Whereas, the second filter layer is a fine filter and is much more efficient on the small particle sizes and considerably more expensive than the

first one. This arrangement allows the operator to replace the lower cost filter more frequently while extending the durability of the high efficiency second-stage filter (Talbert, 2008).

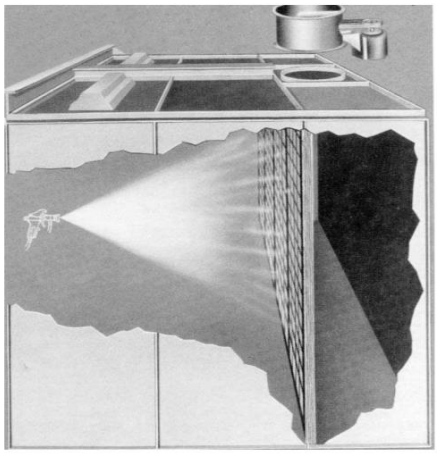

Figure 2-1. Dry filter spray booths (Talbert, 2008)

Water wash booths

A water wash booth composes a curtain of water which flows at the back of the booth or in the floor of the booth. It also has a pump and a sludge separator with chemicals that help to neutralize the coating material. Maintenance of this kind of spray booth is typically higher than a dry filter booth, and the wet sludge collected is a hazardous waste. The primary advantage of a water wash booth over the dry filter spray booth is that the airflow remains constant because the overspray is collected in the sludge where it cannot restrict the exhaust. This also means that production will not be interrupted for any kind of filter change which is necessary in the case of dry filter spray booths, in the middle of the day that usually takes a lot of time to do, in order to minimize the risk of part contamination (Talbert, 2008).

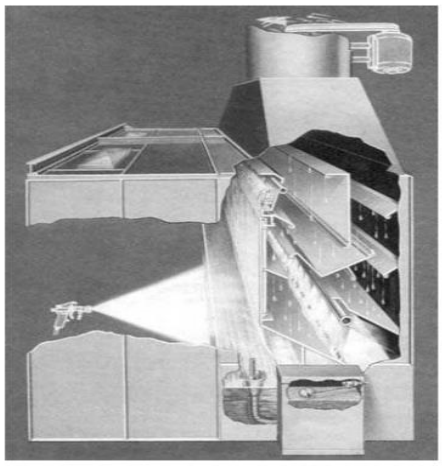

Figure 2-2. Water wash booth (Talbert, 2008)

2.1.2 Options of the direction of air flow

In the spray booth systems, the airflow can be either vertical in a down draft design or horizontal in a cross draft design. In order to contain the paint overspray airflow, it is necessary with which a slight negative pressure is created inside the spray booth (Ron Joseph & Associates, 1991).

Down draft

The air flows from the ceiling of the spray booth vertically downward towards the floor where the exhaust is located. This is usually preferred when the paint operator walks around the part which is more convenient in the case of large machines or vehicles (Ron Joseph & Associates, 1991).

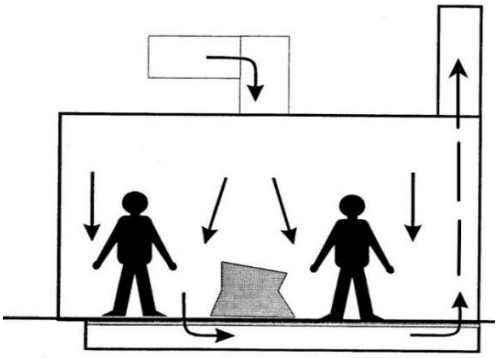

Figure 2-3. Down draft (Ron Joseph & Associates, 1991)

Cross draft

Air flows from behind the operator towards the vertical filter bank or water curtain. The air moves parallel to the floor. This direction is preferred when parts are suspended from a rack or conveyor and the operator applies paint in one direction. Out of all the paint booth types available this is considered to be the least expensive (Ron Joseph & Associates, 1991).

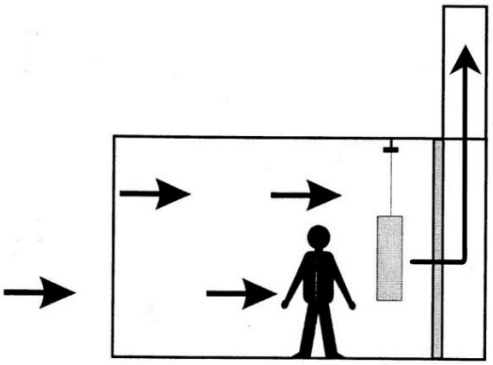

Figure 2-4. Cross draft (Ron Joseph & Associates, 1991)

Semi-down draft

The air travels from the ceiling at the front of the booth towards the floor at the back of the booth where the exhaust is located. Air movement is in a diagonal direction. In an alternate model, the air moves from the ceiling down towards one of two level exhaust plenums located along the side walls of the booth (Ron Joseph & Associates, 1991).

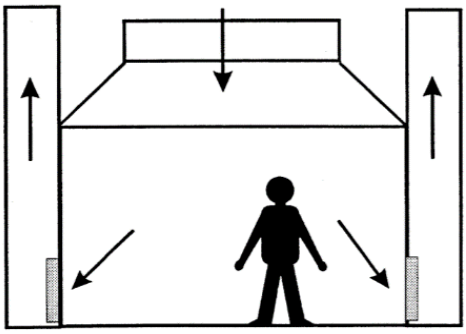

Figure 2-5. Semi-down draft (Ron Joseph & Associates, 1991)

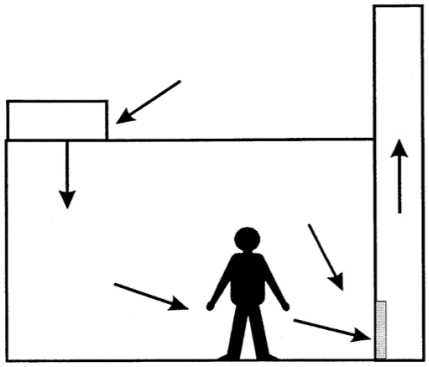

Figure 2-6. Semi-down draft (Ron Joseph & Associates, 1991)

2.2 Computational fluid dynamics (CFD)

Computational fluid dynamics (CFD) is a branch of fluid mechanics that analyses problems involving fluid flow using numerical analysis. It deals with the study of the mechanics of fluids and forces acting on them. In other words, it is the use of applied mathematics, physics and computational software to visualize how a gas or liquid flows and how they affect objects as they flow past them.

CFD in ventilation design is used to predict thermal-fluid physical phenomena. Heat flows like heat conduction through the building enclosure, heat gains from heated objects, and solar radiation through the building facade, phase changes like condensation and evaporation of water contents, chemical reactions like combustion in case of a fire, mechanical movements of fans and occupant movement can be predicted using CFD.

The basic structure followed in computational fluid dynamics has three important steps:

a. Pre-processing
b. Processing or simulation
c. Post- processing

During pre-processing, the geometry and physical boundaries of the problem are designed. The surfaces and the extracted volume are divided into cells or elements known as a mesh. The problem is then defined with the help of boundary conditions, fluid properties, flow models.
In the processing stage, the governing equations are numerically solved either as steady state or transient.
Post-Processing involves extracting the desired flow properties from the computed flow field in the form of numerical values, graphs, contours, directional vectors, etc, and are used for the analysis and visualization of the resulting solution.

2.2.1 Turbulence Modelling

A turbulence model is defined as a set of algebraic or differential equations which determine the turbulent transport terms in the mean flow equations and close the system of equations. All turbulent flows being transient and three-dimensional forces us to develop methods for averaged quantities to extract useful information. One of the methods for dealing with turbulent flows is Reynolds averaging which provides information about the overall mean flow properties.

Reynolds Averaging

The main idea behind Reynolds averaging is to express any variable, $\Phi(x,t)$ which is a function of time and space, as the sum of a mean and a fluctuating component as given by

$$\Phi(x,t) = \bar{\Phi}(x) + \Phi'(x,t) \quad [2.1]$$

where Φ is the instantaneous variable, $\bar{\Phi}$ is the mean and Φ' is the fluctuation component. The idea is that the average has the primary influence and the fluctuation has the secondary influence. The resulting equations using Reynolds decomposition and averaging are called the RANS or Reynolds Average Navier Stokes equations.

However, the Reynolds decomposition and averaging of the Navier-Stokes does not address the closure problem entirely. The non-linearity of the Navier-Stokes equations means that the velocity fluctuations still appear in the RANS equations, in the form of Reynolds stress term also known as turbulent stress. This term requires additional modelling to close the RANS equations. The function of turbulence modelling is to devise approximations for the unknown correlations in terms of flow properties that are known so that a sufficient number of equations exits. By making such approximations we close the system of equations.

Boussinesq was the first to attack the closure problem, by introducing the concept of eddy viscosity by making an analogy between the shear stress and turbulent stress. This reduces the number of unknowns and the turbulence models are further used to tackle the rest of the closure problem.

K-epsilon model

K-epsilon (k-ε) turbulence model is the most commonly used model in the engineering applications of Computational Fluid Dynamics (CFD) to simulate mean flow characteristics for turbulent flow conditions. (ANSYS, 2018). The underlying assumption of this model is that the turbulent viscosity is isotropic, in other words, the ratio between Reynolds stress and mean rate of deformations is the same in all directions. The ststandard k-epsilon$k$-ε) model (Launder & Spalding, 1972) is a semi-empirical model based on model transport equations for the turbulence kinetic energy k [m^2/s^2] and its dissipation rate ε [m^2/s^3].

The turbulence kinetic energy and its rate of dissipation are obtained from the following transport equations:

$$\frac{\partial(\rho k)}{\partial t}+\frac{\partial(\rho k\overline{u_\iota})}{\partial x_i}=\frac{\partial}{\partial x_j}\left[\left(\mu+\frac{\mu_t}{\sigma_k}\right)\frac{\partial k}{\partial x_j}\right]+G_kG_b-\rho\varepsilon-Y_M+S_k \qquad [2.2]$$

and

$$\frac{\partial(\rho\varepsilon)}{\partial t}+\frac{\partial(\rho\varepsilon\overline{u_\iota})}{\partial x_i}=\frac{\partial}{\partial x_j}\left[\left(\mu+\frac{\mu_t}{\sigma_\varepsilon}\right)\frac{\partial\varepsilon}{\partial x_j}\right]+C_{1\varepsilon}\frac{\varepsilon}{k}(G_k+C_{3\varepsilon}G_b)-C_{2\varepsilon}\rho\frac{\varepsilon^2}{k}+S_\varepsilon \qquad [2.3]$$

Where, $\overline{u_\iota}$ is the mean velocity component in the corresponding direction [m/s]

ρ is the density of the fluid [kg/m^3]

In these equations, G_k represents the generation of turbulence kinetic energy due to the mean velocity gradients, calculated as shown in equation [2.4]

$$G_k=-\rho\overline{u_\iota'u_j'}\frac{\partial\overline{u_\iota}}{\partial x_i} \qquad [2.4]$$

G_b is the generation of turbulence kinetic energy due to buoyancy, calculated as shown in equation [2.5]

$$G_k=-g_i\frac{\mu_t}{\rho Pr_t}\frac{\partial\rho}{\partial x_i} \qquad [2.5]$$

Where, g_i is the component of the gravitational vector in the ith direction

Pr_t is the turbulent Prandtl number for energy and has a value of 0.85

Y_M represents the contribution of the fluctuating dilatation in compressible turbulence to the overall dissipation rate, which is irrelevant for the current study as the compressibility of the fluid is not taken into account.

$C_{1\varepsilon}$, $C_{2\varepsilon}$ and $C_{3\varepsilon}$ are constants. σ_k and σ_ε are the turbulent Prandtl numbers for k and ε, respectively. S_k and S_ε are user-defined source terms.

The turbulent viscosity, μ_t, is computed by combining k and ε as shown in equation [2.6]

$$\mu_t=\rho C_\mu\frac{k^2}{\varepsilon} \qquad [2.6]$$

The model constants σ_k, σ_ε, C_μ, $C_{1\varepsilon}$, $C_{2\varepsilon}$ have values are as follows (Launder & Spalding, 1972):

$\sigma_k = 1.00, \sigma_\varepsilon = 1.30, C_\mu = 0.09, C_{1\varepsilon} = 1.44, C_{2\varepsilon} = 1.92$

These values have been determined experimentally with air and water for fundamental turbulent shear flows including homogeneous shear flows and decaying isotropic grid turbulence.

Enhanced wall treatment

Standard k-epsilon (k-ε) turbulence model is not capable of simulating the flow in the vicinity of the wall. This inconsistency is solved by introducing the two layer model. The computational domain is divided in two regions, viscosity affected near wall region and fully turbulent core region. Two different models are used, the complete k-ε model for the outer region and a simplified model one-equation k-based model for the near-wall. The separation between the two regions is defined in terms of a distance from the wall.

Enhanced wall treatment is a near-wall modelling method that combines a two-layer model with so-called enhanced wall functions. If the near-wall mesh is fine enough to be able to resolve the viscous sublayer, then the enhanced wall treatment will be identical to the traditional two-layer model.

However, the restriction that the near-wall mesh must be sufficiently fine everywhere might demand a large computational requirement. It is convenient to have a near-wall formulation that can be used with coarse meshes (usually referred to as wall-function meshes) as well as fine meshes (low-Reynolds-number meshes). In addition, the excessive error should not be incurred for the intermediate meshes where the first near-wall node is placed neither in the fully turbulent region, where the wall functions are suitable nor in the direct vicinity of the wall, where the low-Reynold-number approach is adequate.

To achieve the goal of having a near-wall modelling approach that will possess the accuracy of the standard two-layer approach for fine near-wall meshes and at the same time, will not significantly reduce accuracy for wall-function meshes, ANSYS FLUENT combines the two-layer model with enhanced wall functions (ANSYS, 2018).

2.2.2 Discrete phase model (DPM)

In addition to solving transport equations for the continuous phase, ANSYS Fluent allows to simulate a discrete second phase in a Lagrangian frame of reference. Trajectories of particles/droplets are computed in a Lagrangian frame (ANSYS, 2018).

Purpose of the DPM particles in the uncoupled DPM is for postprocessing, and so particles are not tracked except when requested, to calculate and display particle tracks. In uncoupled DPM the particles do not influence the flow.

In Steady Tracking, as soon as a particle is released it is tracked until it reaches its final destination according to the specified boundary behaviour. Particle boundary conditions at walls, inlets, and outlets are specified as *trap*, *escape* and *reflect* which work as the name implies. Physical properties of the discrete phase are included by enabling the physical model to have the effect of various forces on the particles.

Dispersion of particles due to turbulent fluctuations in the flow is be modelled using stochastic tracking. Each injection is tracked repeatedly in order to generate a statistically meaningful sampling. A random turbulent dispersion is added to each track.

Injections can be defined as cone where particle streams are injected in a conical pattern. Every injection definition includes the particle type whether it is inert, droplet, or combusting particle, material of the particle (from database) and its initial conditions (Bakker, 2018).

2.3 PorZo Tool

ANSYS Fluent allows to model pressure restricting devices like filters otherwise called as a porous material or perforated plates also called flow restrictors, using two choices, by using porous jump and porous zone. In order to define these choices, we need to specify face permeability [m^2] and inertial resistance coefficient, C2 [1/m].

Often times it is difficult and time taking to obtain these parameters for which PorZo was used to simplify this calculation process. PorZo is an ACT Extension for ANSYS Fluent written in IronPython with table or text file based inputs of measured data with which Porous Jump and Porous Zone are set up (Vondál, 2018).

The porous media and porous jump can be defined using two options.

1) Flow Restrictor
2) Thin Perforated Plate

2.3.1 Flow Restrictors (Filters, Porous zones, Porous Jumps)

Two types of flow restrictors can be specified:

1) Thin restrictor represented by 2D surface. Filter is simplified into 2D surface with porous jump procedure.
2) Thick restrictor represented by 3D zone. Porous zone definition for a complex 3D zone with directional pressure loss anisotropy is employed.

Flow Restrictor Input Definition

By choosing restrictor type required inputs are defined. Required inputs are:

1) Cell Zone name – name of cell zone is given. The given cell zone has to be of type "*fluid*".
2) Directional dependence – direction is specified if the pressure loss is anisotropic by choosing *Yes* or independent of direction if the pressure loss is isotropic by choosing *No*.
3) Choose filter – predefined filter with no additional inputs can be chosen or Custom filter where the additional specification is required and all the data has to be provided.
4) Choose data input method - in case of custom filter specification user can import data of filter either from the file or create Table. Inputs have to be in a form velocity [m/s] x pressure [Pa].

2.3.2 Thin Perforated Plates

Four types of thin perforated plates can be predicted:

1) General shape
2) Generic Staggered Arrangement
3) Square Arrangement
4) 60° Offset Staggered Arrangement

Perforated Plates Input Definition

While choosing the Perforated Plates option in PorZo wizard, it is required to provide several inputs:

1) Velocity [m/s] – bulk velocity in front of plate.
2) Pipe diameter [m] – channel hydraulic diameter where the plate is placed.
3) Density [kg/m^3] – the density of the fluid when experimental pressure loss was obtained.
4) Dynamic viscosity [kg/m-s] – viscosity of the fluid when experimental pressure loss was obtained.
5) Choose method and plate –
    - General shape
    - Generic Staggered Arrangement
    - Square Arrangement
    - 60° Offset Staggered Arrangement
5) Surface name – The name from boundary conditions has to be given which is to be considered as the perforated plate. Surfaces have to be of type *Interior* or *Wall* with fluid on both sides.
6) Generic Staggered Arrangement

Required inputs are:

a. Hole distance 1 [m] – distance between two horizontal holes (from centre to centre)
b. Hole distance 2 [m] – distance between two vertical holes (from centre to centre)
c. Hole diameter [m] – hole diameter has to be specified.

2.4 Spray painting

Spray painting is a painting technique that uses a device, usually a spray gun shown in Figure 2-7, to spray the paint onto a surface of an object. The bulk paint liquid is atomized into small droplets with the help of this spray gun. A spraying system usually comprises a pump to pressurize the paint and pump it through the hose to the spray gun.

Figure 2-7. Spray gun (Jicolor, 2018)

Spray systems are mainly of four types

1. Airless
2. Conventional
3. Electrostatic
4. High volume low pressure

The main function of all these types of spray systems is to atomize the paint and spray it onto the object.

Airless spray system

As the name implies the airless system does not require air to atomize the paint. These operate at 3.5 – 34.5 MPa pressure to atomize the coating, using different tip sizes to achieve the desired atomization and spray pattern size. Of all the systems the most widely used system is the airless system (pati, 2018).

Conventional spray system

It uses high velocity air jets to produce a very high atomization power. Air pressure inside the air cap during use is typically 200 to 400 kPa with an air volume consumption of 170 to 700 l/min.

Electrostatic spray system

In electrostatic spray painting, the atomized particles are electrically charged which makes them to repel with each other and spread themselves evenly as they exit the spray nozzle.

High volume low pressure

It uses larger air volumes at low Pressure to atomise the coating. It has a higher transfer efficiency than conventional air atomizing due to the lower pressure air. However, the droplet sizes produced tend to be slightly larger which sometimes results in a lower quality finish (CJ Coatings UK, 2018).

3. Proposed design and variations

3.1 Model Design

The spraying booth selected to analyse can be called as a portable spraying booth with approximately one cubic meter volume which is obtained from a research report (Zelenský & Švandová, 2018). This can be used in spray painting of small parts.

Figure 3-1. Model Design

The main parts of the spraying booth comprise:

1. Front box: This is where the parts are spray painted. It can be called as the working space.
2. Perforated plate: The front box has a perforated plate at the bottom dividing the working space into two. The bottom space has a slope to drain the paint reducing the probability of getting stuck to the walls.
3. Rear box: The rear box works as the exhausting chamber to which the exhaust fan is connected.
4. Pedestal: All the parts are together fixed on a pedestal for the convenience of the worker.

5. Filter: The filters separate the front from the rear box which collect the over sprayed paint particulates which were not deposited on the surface to be painted.

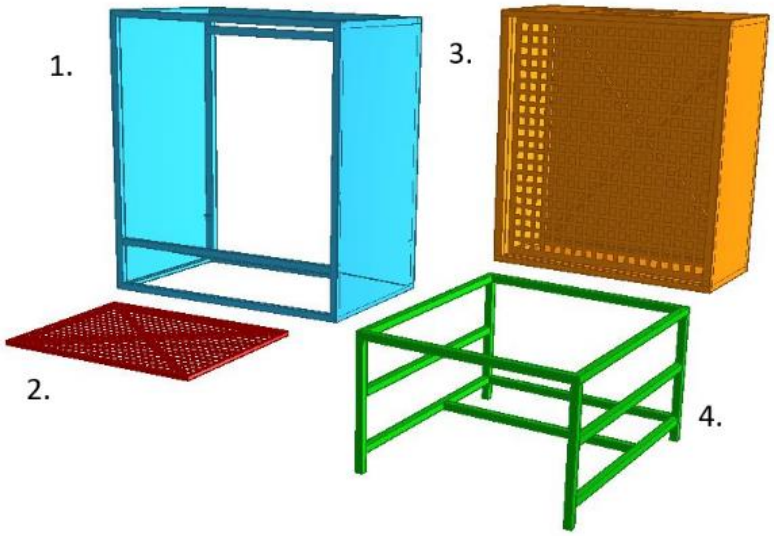

Figure 3-2. Parts

However, all the parts are not necessary to analyse. The only parts required in CFD are the front box, filter and the rear box. So, the geometry was cleaned up using Autodesk Inventor, removing the irrelevant elements like pedestal stand and some frames and various options of exhaust ventilation (outlets) and also included the inlets in the front box.

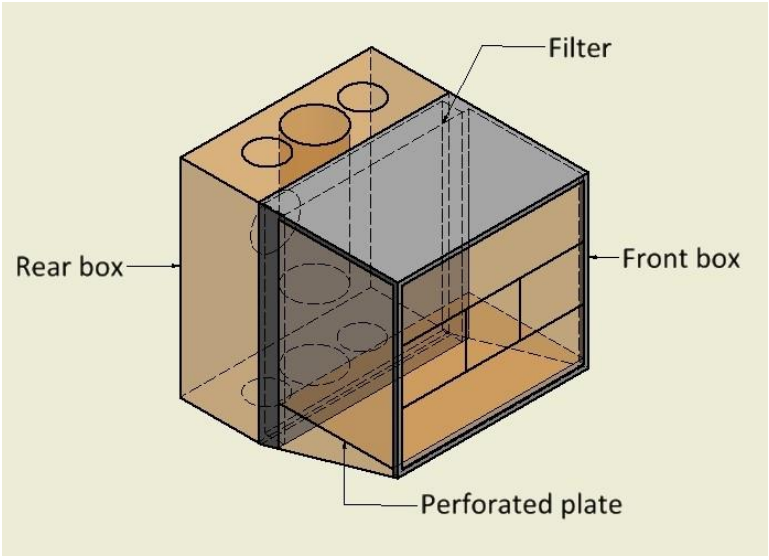

Figure 3-3. Cleaned up model

3.2 Design variations

As mentioned before, the rear box serves as the exhausting chamber to which the exhaust fan is connected. Circular openings are placed at different positions of the rear box in order to analyse the best option to exhaust the extracted air. The various placements of the outlets in the rear box can be seen in Figure 3-4.

3.2.1 Outlet options

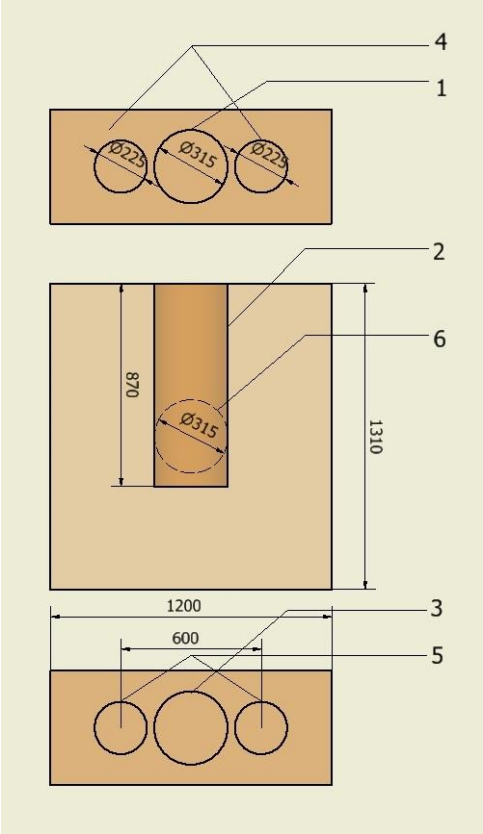

Figure 3-4. Outlet options

1. Circular opening with 315mm diameter in the top surface in the centre.
2. Circular opening with 315mm diameter in the top surface in the centre with a pipe of the same diameter inserted into the rear box and length 870mm which is two thirds of the height of the rear box.
3. Circular opening with 315mm diameter in the bottom surface in the centre.
4. Circular opening with 315mm diameter in the rear surface in the centre.
5. Two circular openings with 225mm diameter in the top surface on either side 600 mm apart from each other.

6. Two circular openings with 225mm diameter on the bottom surface on either side 600 mm apart from each other.

3.2.2 Inlet options

A few inlet options for the front box are also placed to analyse the best option. These inlet options can be seen in Figure 3-5.

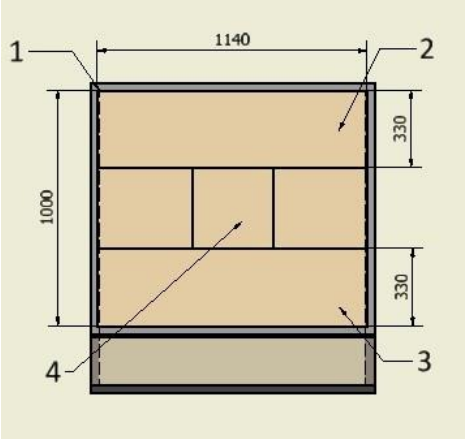

Figure 3-5. Inlet options

1. The front opening on the front box with dimensions 1140 mm x 1000 mm.
2. Closable opening on the top of the front inlet with dimensions 1140 mm x 330 mm
3. Closable opening on the bottom of the front inlet with dimensions 1140 mm x 330 mm
4. The square in the middle is made in order to employ it as a source of paint spray.

3.3 Filter

The model contains two filters placed in series in between the front box (working space) and the rear box. The filters used in the model are manufactured by KS Klima Service.

3.3.1 VS LAK Filter

The VS LAK filter is most often used in the first filtration stage and it captures aerosols of excess paint (so-called paint fog), including dry paint or varnish particles. Filtration class of this filter according to EN 779:2012 is G3.

Figure 3-6. VS LAK filter (KS Klima Service, 2014)

It is made with a filter media from glass fibres randomly arranged with high elasticity and low compressibility. This elastic structure of the medium provides a high absorbing capacity of the filter and encourages the operating safety of mounted filters. The medium contains also a special binder that binds excess paint containing a high portion of water component (KS Klima Service, 2014).

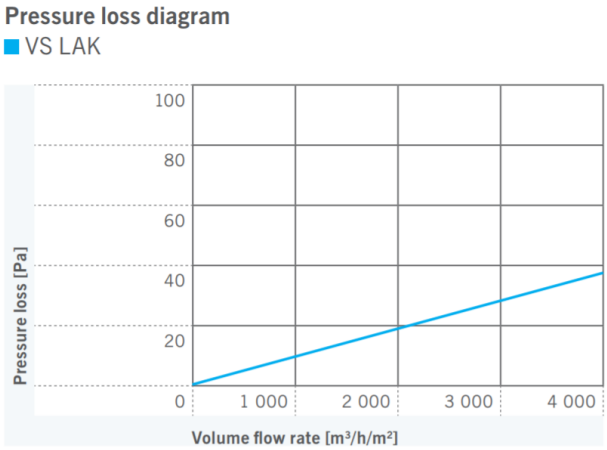

Figure 3-7. VS LAK filter - Pressure loss diagram (KS Klima Service, 2014)

3.3.2 KS PA Grün 4" filter

The KS PA Grün 4" filter is used in particular for adsorption of paint aerosols as so-called floor filters in spraying boxes. Filtration class of this filter according to EN 779:2012 is G4.

Figure 3-8. PA 4" filter (KS Klima Service, 2014)

It is made from progressively thickened and highly elastic, non-flammable glass fibres. The material features a high paint aerosols accumulation capacity from 3,500 to 5,900 [g/m^2]. (KS Klima Service, 2014)

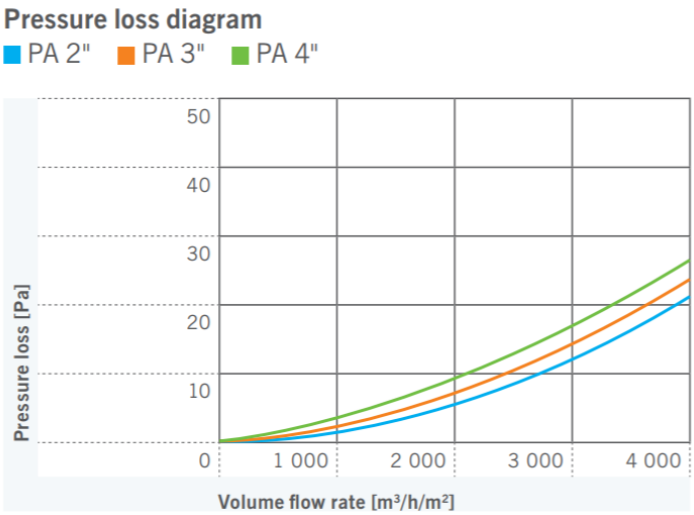

Figure 3-9. PA 4" filter - Pressure loss diagram (KS Klima Service, 2014)

3.3.3 VS LAK + PA Grün 4" pressure loss

As the two filters VS LAK and PA 4" are stacked in series, the pressure losses of both the filters are supposed to be added in order to determine the pressure losses at different volume flow rates for both the filters together. Using the pressure loss diagrams (see Figures 3-7 and 3-9) of the individual filters the combined values were determined as below.

Table 3-1. VS LAK + PA Grün 4" pressure loss

$\dot{V}$ [m³/h/m²]	u [m/s]	PA-4" ΔP_{loss} [Pa]	VS-LAK ΔP_{loss} [Pa]	Total ΔP_{loss} [Pa]
0	0	0	0	0
500	0.14	1.3	5.0	6.3
1000	0.28	3.7	9.6	13.3
1500	0.42	6.3	14.6	20.9
2000	0.56	9.3	18.9	28.2
2500	0.69	12.8	23.6	36.3
3000	0.83	16.9	28.1	45.0
3500	0.97	21.3	32.9	54.2
4000	1.11	26.5	37.4	63.8

Using the calculated values, with the help of MS Excel a curve was generated as shown in Figure 3-10.

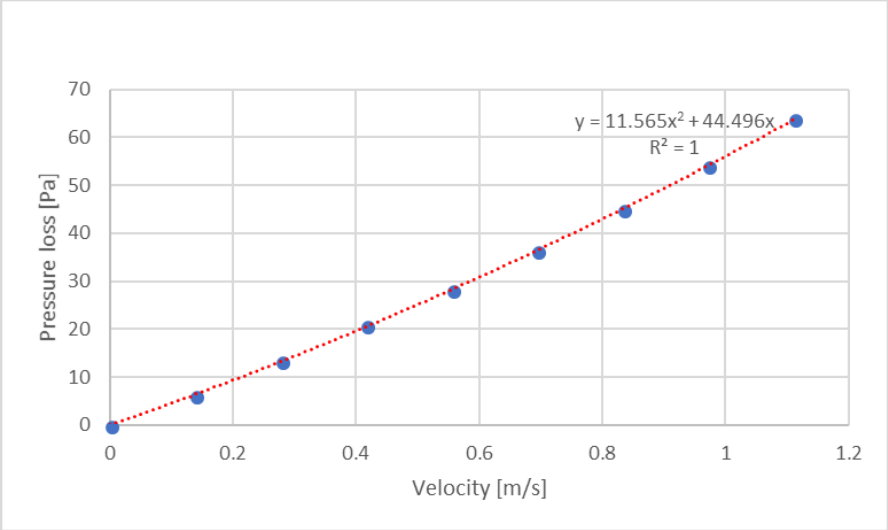

Figure 3-10. VS LAK filter + PA Grün 4" filter pressure loss diagram

From the curve's trendline a polynomial equation [3.1], was generated for the curve. Using equation [3.1], various pressure loss values for respective velocities were determined which were used in the PorZo, as inputs to define the 3D porous media.

$$\Delta P_{loss} = 11.565\, u^2 + 44.496\, u \qquad [3.1]$$

Where, ΔP_{loss} is Pressure loss [Pa]

u is velocity [m/s]

3.4 PorZo application

PorZo tool was used to model pressure restricting devices in the model which are the filters (VS LAK filer + PA Grün 4" filter), as a single porous zone and perforated plate as a porous jump.

3.4.1 Model inputs

Flow Restrictors

In the model the 3D filter media is defined using the thick flow restrictor represented by 3D zone for which the following inputs were given:

Table 3-2. Custom filter data input

Trendline Equation $\Delta P_{loss} = 11.565\,u^2 + 44.496\,u$	
Velocity [m/s]	Pressure loss [Pa]
0.00	0.0
0.10	4.6
0.15	6.9
0.20	9.4
0.25	11.8
0.30	14.4
0.35	17.0
0.40	19.6
0.45	22.4
0.50	25.1
0.55	28.0
0.60	30.9
0.65	33.8
0.70	36.8
0.75	39.9
0.80	43.0
0.85	46.2
0.90	49.4
0.95	52.7
1.00	56.1

1) Cell Zone name – filter
2) Directional dependence – Direction if the pressure loss is given independent i.e., isotropic by choosing *No*.
3) Choose filter – Custom filter for which all the additional specification data was provided.

4) Choose data input method – Inputs were given in a form velocity [m/s] x pressure [Pa] with the help of table method as shown in table 3-2. Using equation [3.1], the values determined were used in the PorZo tool, as inputs to define the 3D porous media.

Perforated Plate

The perforated plate in the model whose dimensions are 1.20 m x 0.72 m has squared holes of side 0.01 m and the distance between each of them is 0.01 m as well. The percentage of the area can be given by equation [3.2] as 51%.

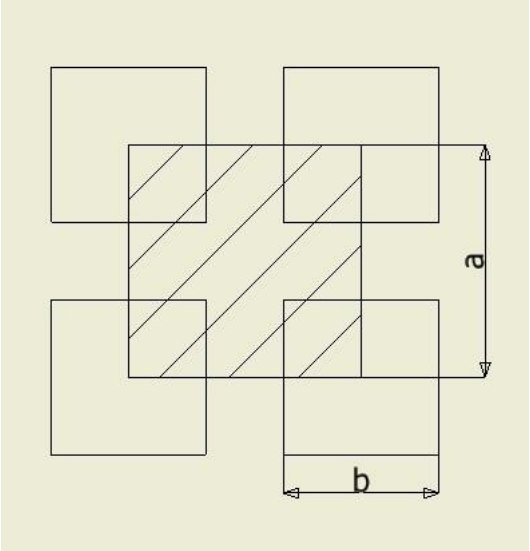

Figure 3-11 Arrangement of holes

$$Percentage\ of\ area = \frac{S_{open}}{S_{gross}} = \frac{b^2}{a^2} * 100\ [\%] \qquad [3.2]$$

Where, b = side of the squared hole [m]

a = distance between the centres of two holes [m]

S_{open} = Surface area of the holes [m^2]

S_{gross} = Surface area without holes [m^2]

In the CFD model, the perforated plate was defined using the Perforated Plates option in PorZo wizard and several inputs were given

1) Velocity = 0.5 m/s

2) Pipe diameter = 0.9 m,

Pipe diameter is the channel hydraulic diameter where the porous zone is placed. The porous zone is placed in the perforated plate whose dimensions are 1.20 m x 0.72 m whose hydraulic diameter was calculated using the equation [3.3].

$$d_h = \frac{2pl}{p+l} \quad [3.3]$$

Where, d_h = hydraulic diameter

p = 1.20 m, the width of the perforated plate

l = 0.72 m, the length of the perforated plate

3) Air density = 1.2 kg/m^3

4) Air dynamic viscosity = 1.815 x 10^{-5} kg/m-s

5) Choose method and plate - Generic staggered arrangement is relevant to the model in this project. But the arrangement in the perforated plate of the model is not staggered as in Figure 3-11. Hence, the arrangement was converted into staggered mathematically as in Figure 3-12.

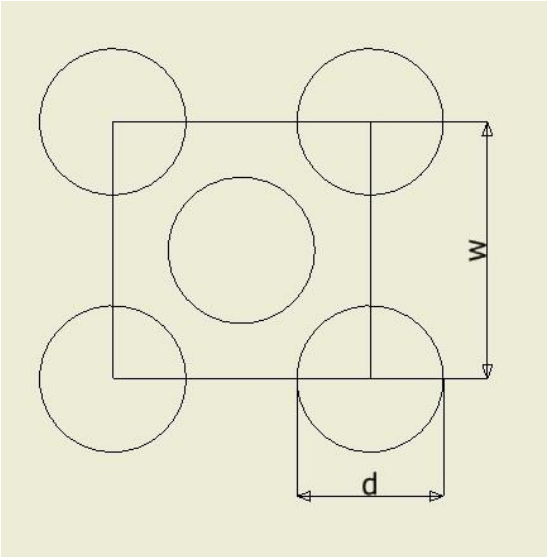

Figure 3-12. Staggered arrangement

The square hole in the actual arrangement is converted into a circular hole using equation [3.4], where a and b are the sides of the square which are the same and are equal to 0.01 m. The distance between the circular holes is calculated as follows,

$$Percentage\ of\ area = \frac{S_{open}}{S_{gross}} = \frac{2\frac{\pi d^2}{4}}{w^2} * 100\ [\%] \quad [3.4]$$

Where, d = diameter of the circular hole [m]

w = distance between the centres of two holes [m]

S_{open} = Surface area of the holes [m^2]

S_{gross} = Surface area without holes [m^2]

In order to calculate we equate equations [3.2] and [3.4] as shown in equation [3.5] as both of the equations give us the percentage of the area which is the same in both the arrangements.

$$Percentage\ of\ area = \frac{S_{open}}{S_{gross}} = \frac{b^2}{a^2} = \frac{2\frac{\pi d^2}{4}}{w^2} * 100\ [\%] \qquad [3.5]$$

Which gives us the value of w as 0.0174 mm.

Required inputs are:

a. Hole distance 1 = 0.0175 m
b. Hole distance 2 = 0.0175 m
c. Hole diameter = 0.01 m

6) Surface name – perforated_plate

3.4.2 PorZo verification

After PorZo was used to model the pressure restricting devices in the model (*VS LAK filer + PA Grün 4" filter, modelled as a single porous zone and perforated plate modelled as porous jump*) by giving the relevant inputs, the simulation was carried out using the velocity outlet, in the exhaust variation with top centre opening in the rear box i.e., the exhausting chamber in order to verify if the pressure restricting devices are working as they are supposed to.

The simulation was carried out with the lowest possible inlet velocity of 0.5 m/s, from which the velocity magnitude for the exhaust was calculated as 7.314 m/s. Velocity inlet with velocity magnitude of 7.314 m/s, in the direction normal to the exhaust, was taken as exhaust boundary condition. The standard k-ε model was used as the turbulent model. After simulating the model with the mentioned conditions the following results were generated.

In the figure 3-13, We can observe a smooth transition of the negative static pressure from the front box to the rear box due to the presence of the filters in between them. The negative static pressure is more in the rear box compared to the front box which is how it is supposed to work in reality. So, we can assume that the porous media created using PorZo is working accordingly.

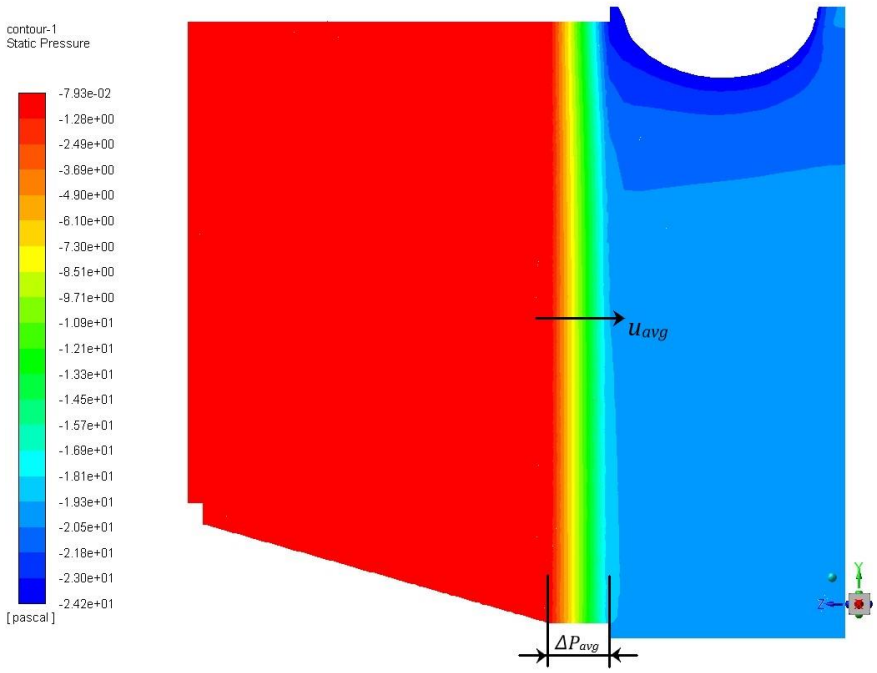

Figure 3-13 Static pressure contour in the model

In Figure 3-14 we can see the sudden pressure drop in the bottom due to the presence of the perforated plate which means that the porous jump created using PorZo is functioning as expected.

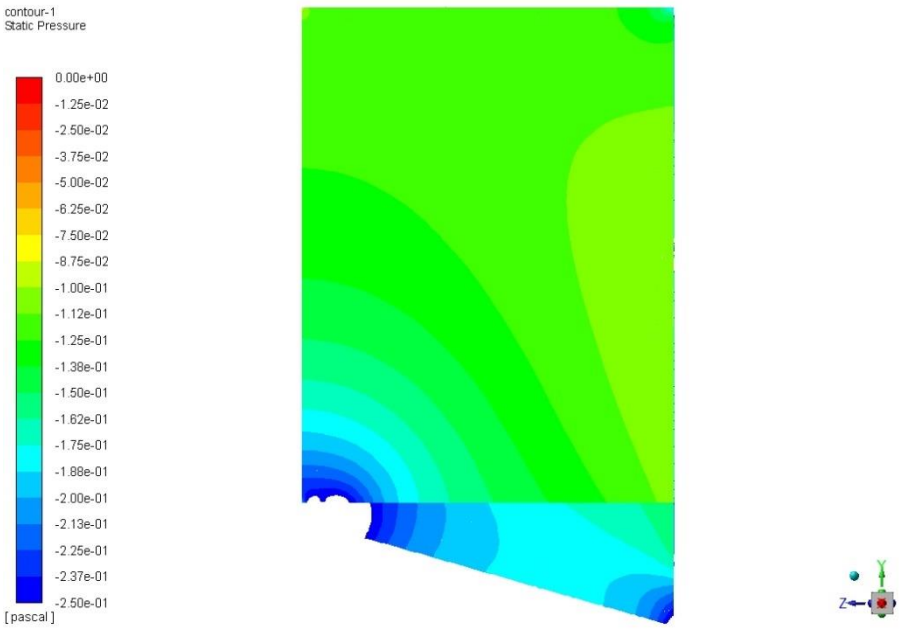

Figure 3-14 Static pressure contour in the working space

Calculation

A calculative verification was also made by comparing the average pressure losses across the filters at an average velocity in front of the filters, from the graph generated for the two filters VS LAK and PA 4" are stacked in series in Figure 3-10, and the results generated by ANSYS Fluent.

Fluent results:

Average velocity in front of the filter, u_{avg} = 0.412 m/s

Average pressure loss in front of the filter = - 0.109 Pa

Average pressure loss in front of the filter = - 20.078 Pa

Average pressure loss of the filter, ΔP_{avg} = - 19.969 Pa

Pressure loss graph

Using the equation 3.1, generated from the graph in Figure 3-10, the same average velocity of 0.412 m/s gives an average pressure loss of 20.295 Pa. It can be seen that the PorZo value is in the vicinity of the Fluent value. The small difference seen is because of considering the average values of the velocity and the pressure on the filter front and rear face. One more reason can be that the front face is divided by the perforated plate at the bottom

4. Meshing

4.1 First cell height

The global mesh resolution parameters will be influenced by this near-wall mesh as well as the Reynolds number. During the pre-processing stage the first cell height, $2y$ was estimated so that the dimensionless distance from the wall, y^+ falls within the desired range. The computed flow-field will dictate the actual y^+ value which in reality will vary along the wall.

The first cell height (2y) near the wall was calculated with the help of equation [4.1].

$$y = \frac{y^+ . \nu}{u_\tau} \quad [4.1]$$

Where, y^+ value is the dimensionless distance from the wall

ν is the kinematic viscosity [m^2/s]

u_τ is the friction velocity [m/s]

The friction velocity, u_τ was calculated using the wall shear stress, τ_w in equation [4.2]

$$u_\tau = \sqrt{\frac{\tau_w}{\rho}} \quad [4.2]$$

Where, τ_w is the wall shear stress [Pa]

ρ is the density of fluid [kg/m^3]

The wall shear stress was calculated using the skin friction coefficient in equation [4.3]

$$\tau_w = C_f . \frac{1}{2} \rho . {u_\infty}^2 \quad [4.3]$$

where, u_∞ is the velocity in the inlet of the model [m/s]

The skin friction coefficient, C_f was calculated using equations [4.4] and [4.5].

a. Laminar flow: Blasius solution (White, 1999)

$$C_f = \frac{0 \cdot 644}{\sqrt{\mathrm{Re}}} \quad [4.4]$$

b. Turbulent flow: Prandtl's one-seventh-power law (White, 1999)

$$C_f = \frac{0.027}{Re^{1/7}} \quad [4.5]$$

The skin friction coefficient, C_f calculated using equations [4.4] and [4.5] applies for boundary layer on a flat plate which is relevant for our case, as all the walls of the model can be considered as flat plates.

The Reynolds number for a flat plate for the model, based on the characteristic length of geometry was calculated using equation [4.6].

$$Re = \frac{u_\infty . x}{\nu} \quad [4.6]$$

where, x is the distance along the wall of the section [m]

ν is the kinematic viscosity [m^2/s]

4.1.1 Front box

The front box, where the flow was expected to be turbulent due to the presence of the worker and the working equipment, the y^+ value was estimated as 1 and the first cell height ($2y$) was calculated using all the formulae mentioned above as 0.2 mm

Table 4-1. Dimensionless distance for the front box

u_∞ [m/s]	Depth [m]	C/S area [m^2]	*Re* [-]	C_f [-]	u_τ [m/s]	y^+ [-]	*Y* [mm]	*2y* [mm]
2.5	0.75	1.14	125000	0.00505	0.126	1	0.119	0.238

Using the calculated first cell height ($2y$), the front box was meshed using the ANSYS Fluent meshing as shown in Figure 4-1, so that the first cell height is the finest which was given the value 0.2 mm and is gradually increased towards the core.

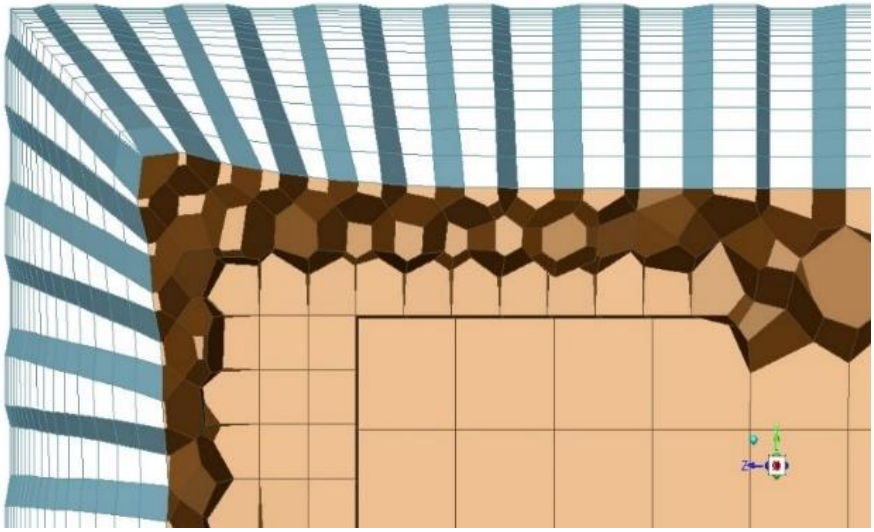

Figure 4-1. Fine mesh near the wall

4.1.2 Rear box

In case of the rear box, where the flow is not as important for this study compared to the front box as we are focusing on the velocity field in the front box, the y^+ value was estimated as 50 and the first cell height was calculated using the above mentioned formulae as 45 mm but due to the inadequacy of space to incorporate enough number of cells in the rear box the cell size was reduced to 30 mm considering the reason that in the analysis the front box is more important.

Table 4-2. Dimensionless distance for the rear box

u_∞ [m/s]	$\dot{V}$ [m³/s]	C/S area [m²]	$\bar{u}_\infty$ [m/s]	Depth [m]	*Re* [-]	C_f [-]	u_τ [m/s]	y^+ [-]	*Y* [mm]	*2y* [mm]
0.5	0.57	0.588	0.97	1.31	84660	0.00228	0.033	50	22.9	45.8

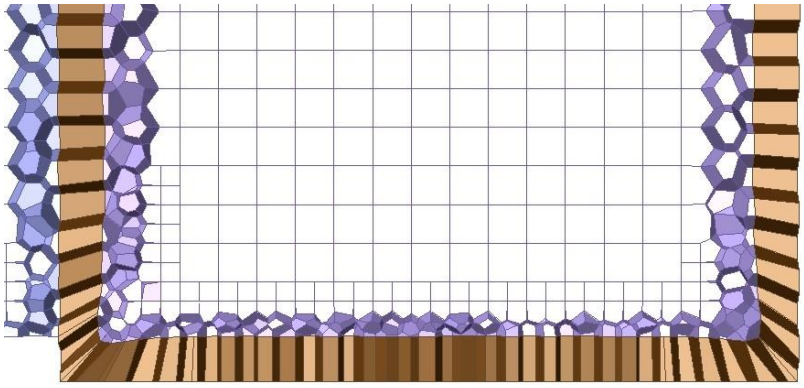

Figure 4-2. Coarse mesh near the wall

Using the calculated first cell height ($2y$), the rear box was meshed using the ANSYS Fluent meshing as shown in Figure 4-2, so that in the above mesh that the first cell height is the same as it is in the core which was given as 30 mm for obtaining a better looking mesh which wouldn't be possible if it was given 45 mm.

Hexcore is a hybrid meshing scheme that generates tet cells adjacent to triangular boundary meshes and a Cartesian mesh in the core flow regions as seen in Figure 4-3. When there is a large disparity in size distribution between the boundary mesh and the initial Cartesian cells, there will be a rapid transition from fine to coarser cells. This controlled by the buffer layers and peel layers.

As shown above, using the first cell height values the volume mesh was developed as shown in Figure 4-3.

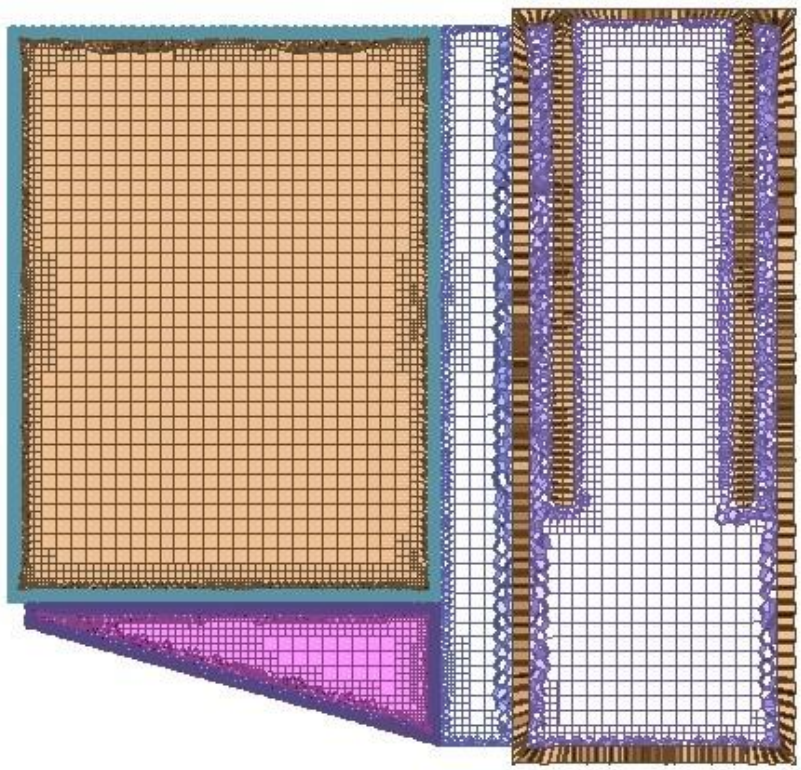

Figure 4-3. Cross-section of volume mesh of the model

5. Boundary Conditions

5.1 Exhaust outlet

In order to decide the right type of outlet for the exhaust, a comparative study was made by choosing different types of the outlet and both laminar and turbulent models (k-ε) were simulated and the convergence and the behaviour of the velocity vectors at the outlet were observed.

The inlet velocity is advised to be in the range of 0.5 – 2.5 m/s (Hejma et al., 1981) and the inlet in the front box is 1 m x 1.14 m and density of air ρ was taken as 1.2 kg/m^3. From which the volumetric flow rate and mass flow rate ranges were calculated.

Table 5-1. Mass flow rate range

Inlet Velocity, $\boldsymbol{u}_\infty$ [m/s]	0.5	2.5
Volumetric flow rate, $\dot{\boldsymbol{V}}$ [m^3/s]	0.57	2.85
Mass flow rate, $\dot{\boldsymbol{m}}$ [kg/s]	0.684	3.42

5.1.1 Mass flow outlet

The laminar model was chosen with the mass flow outlet with mass flow rate as 0.648 kg/s and was simulated with the following residuals.

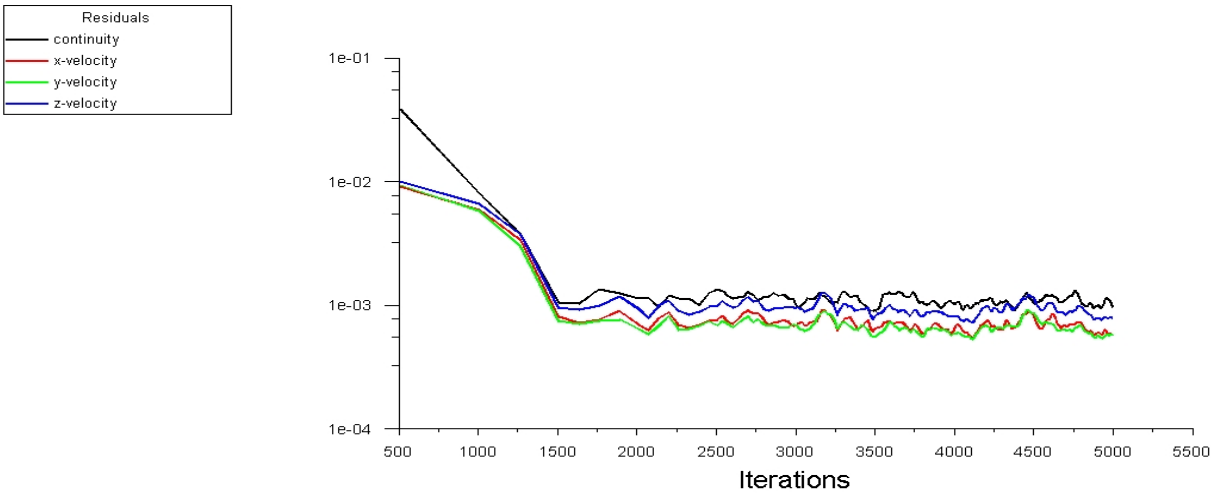

Figure 5-1. Mass flow outlet

5.1.2 Velocity outlet:

The laminar model was chosen with the outlet velocity 14.623 m/s and was simulated with the following residuals.

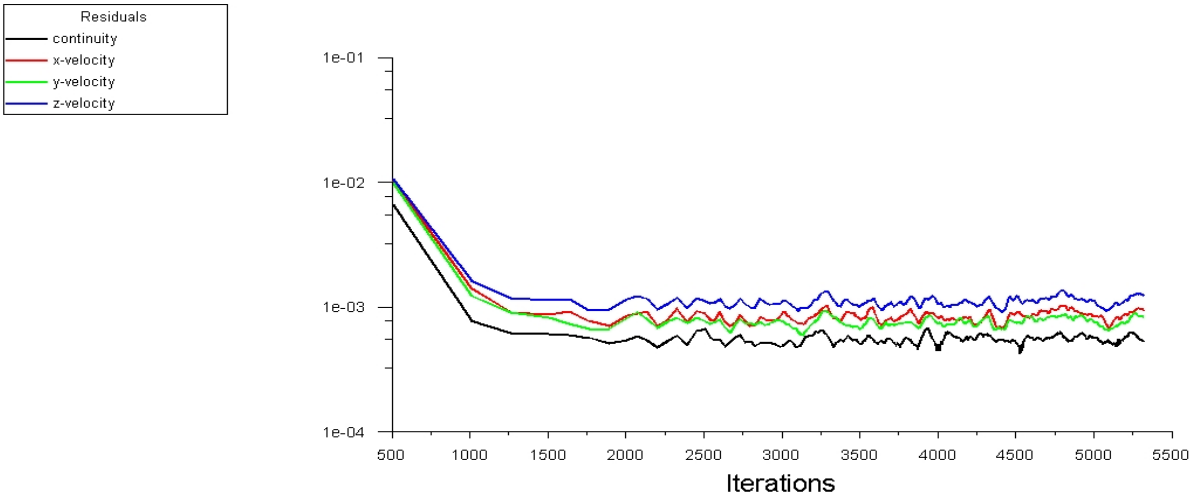

Figure 5-2. Velocity outlet-Laminar model

Turbulence model with the same outlet velocity 14.623 m/s and was simulated with the following residuals.

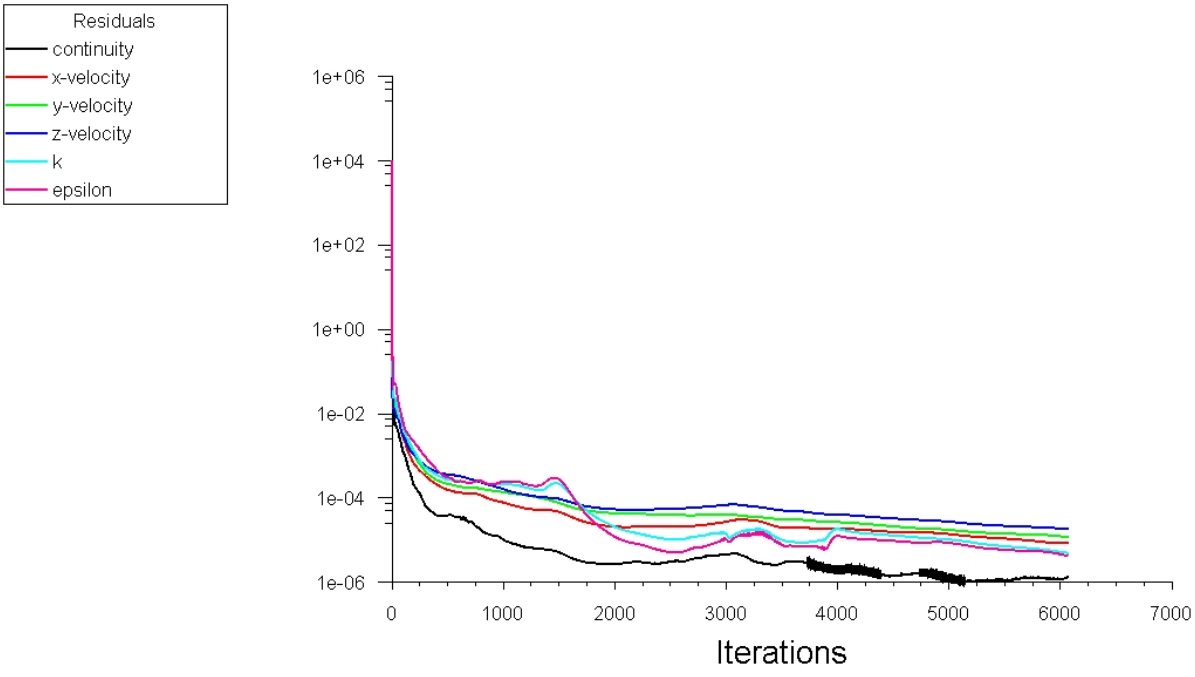

Figure 5-3. Velocity outlet-Turbulent model

From the residuals, we can observe that the turbulence model has better convergence than the laminar model. This is because the laminar model is not capable of capturing any kind of turbulence that occurs in the model.

The velocity vectors at the exhaust can be seen to be at an angle from the exhaust. This phenomenon is quite natural because the air is being sucked out of a small exhaust into a larger ambience which gives this shape to the velocity vectors at the exhaust.

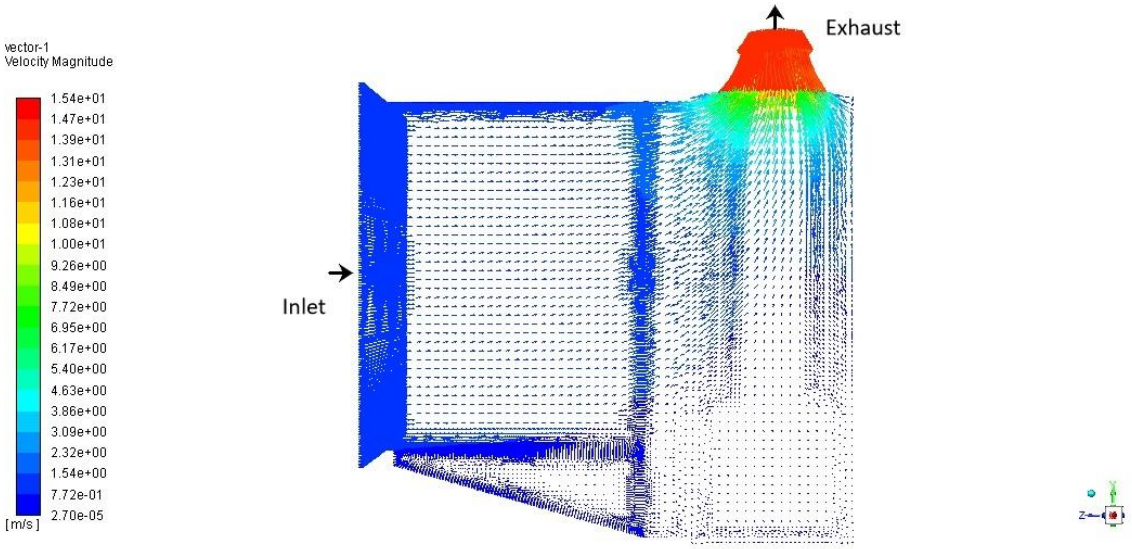

Figure 5-4. Velocity vectors

All of the above simulations were made without any filter media. In order to include the filter media in the model for further study, an ACT software called PorZo was used and the simulations were performed using the velocity outlet and a turbulence model.

6. Results

In order to decide the best option to place the exhaust, all the six variations were simulated for both the highest inlet velocity and the lowest. Further to improve the velocity magnitude in the working space, the cases with a closable opening on the top of the front inlet with dimensions 1140 mm x 330 mm were also simulated.

6.1 Lowest inlet velocity

A total of 6 outlet variations as shown in Figure 3-4, were simulated with the lowest option for the inlet velocity which is 0.5 m/s. All though the inlet velocity is the same in all the cases, in order to generate this inlet velocity with different outlet options, different exhaust velocities are required depending on the surface area of the outlet. The following table shows the velocity magnitude for all the outlet options used (see Figure 3-4).

Table 6-1. Velocity magnitude for outlet variations with the lowest inlet velocity

Outlet option	**Inlet velocity [m/s]**	**Inlet surface area [m^2]**	**Inlet volume flow rate [m^3/s]**	**Diameter of the outlet [m]**	**Outlet surface area [m^2]**	**Exhaust velocity [m/s]**
1	0.500	1.140	0.570	0.315	0.0779	7.314
2				0.315	0.0779	7.314
3				0.315	0.0770	7.314
4				0.315	0.0779	7.314
5				2 X 0.225	0.0795	7.168
6				2 X 0.225	0.0795	7.168

The simulations were carried out using velocity inlet with the respective velocity magnitude according to the table 6-1, in the direction normal to the exhaust was taken as exhaust boundary condition. The standard k-ε model was used as the turbulent model. After simulating the models the following results were generated.

6.1.1 Velocity vectors

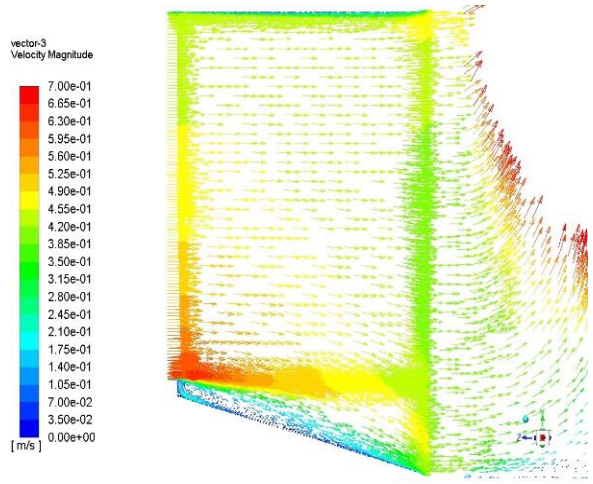

Figure 6-1.Velocity vectors of top centre opening (option 1)

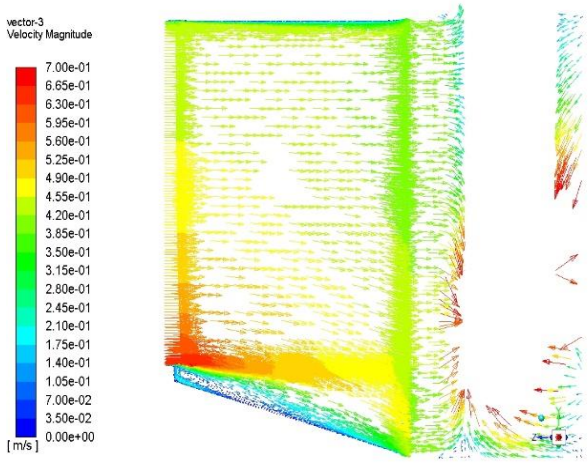

Figure 6-2.Velocity vectors of top centre opening with inserted pipe (option 2)

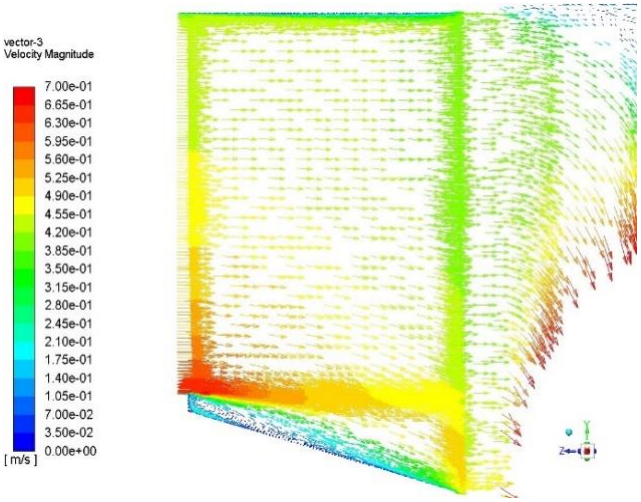

Figure 6-3. Velocity vectors of bottom centre opening (option 3)

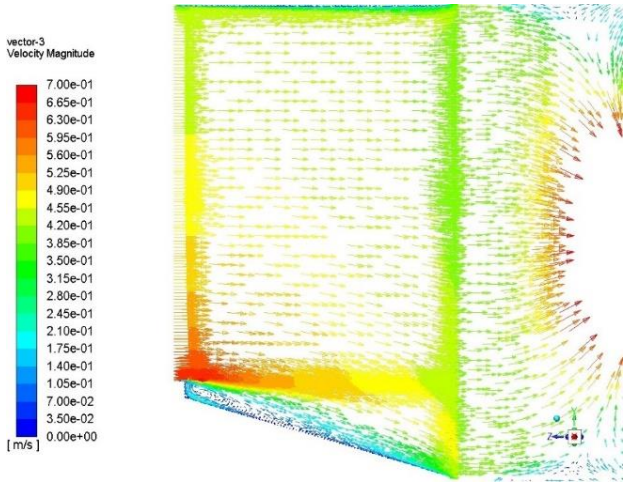

Figure 6-4. Velocity vectors of the rear opening (option 4)

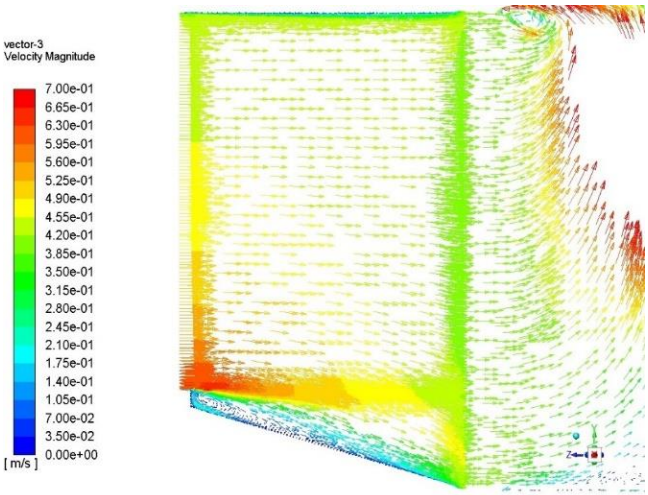

Figure 6-5. Velocity vectors of top right and left openings (option 5)

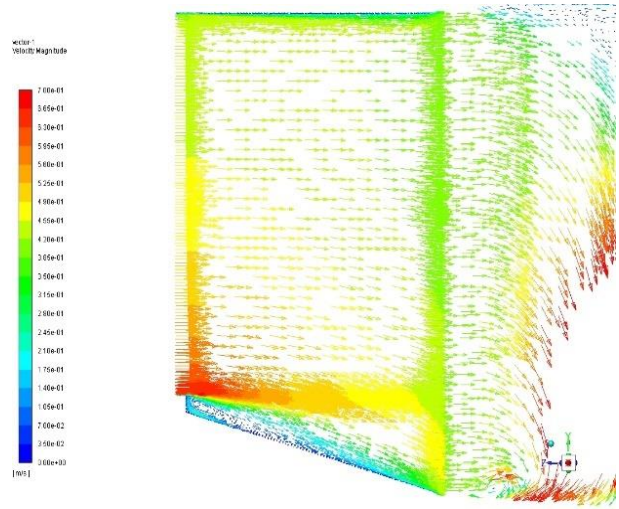

Figure 6-6. Velocity vectors of bottom right and left openings (option 6)

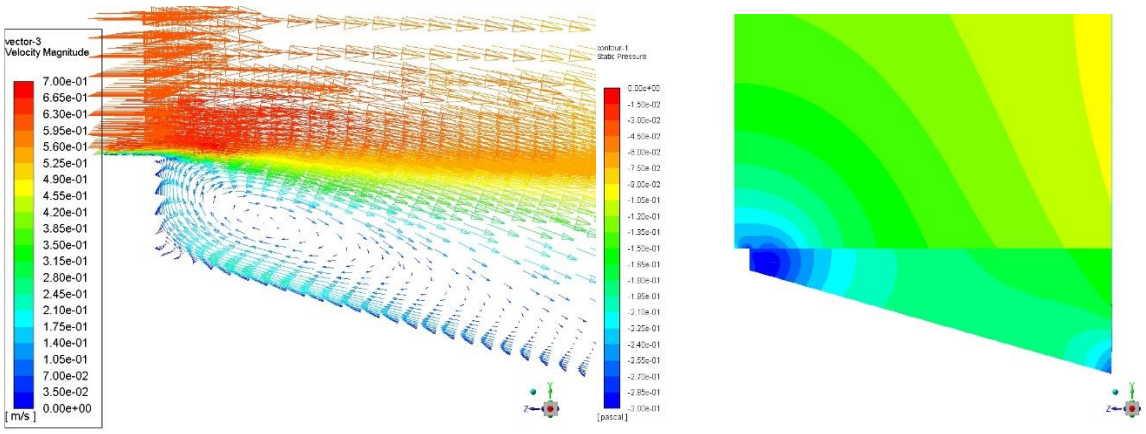

Figure 6-7. Close up of velocity vectors and pressure field the vortex

It can be seen that the velocity vectors in all the cases look quite similar to one another. This is because the velocities in the working section are quite low. The flow pattern is quite uniform due to the presence of the filters between the rear box and the front box, which act as flow restrictors reducing the velocity magnitude in the working space. This makes the chance to see any changes in the velocity field in the working section low.

But, it can be observed in Figure 6-7, that in the bottom of the working space just below the perforated plate a vortex is formed. This recirculation is caused because of the low pressure in this area, the air returns to the top working space through the perforated plate which can cause the paint particles to return into the working space again. Looking at the velocity vectors of all these cases it hard to decide the best option just yet.

6.1.2 Velocity contours

If the velocity magnitude contours in all the cases are observed, it can be seen that in the first three options in Figures 6-8, 6-9 and 6-10, the velocity magnitude is not uniform in the filter region. This can be a problem as the filters can be clogged with particulates only in some locations and this in turn can disturb the velocity field in the working space causing irregularities in the air flow pattern. Whereas, in case of the rear opening as seen in Figure 6-11 and top right and left openings shown in Figure 6-12 a desirable uniform velocity magnitude in the filter vicinity can be seen. This means that so far from the results obtained, these two options seem to be better than the rest if the uniformity of velocity over the filter region is considered as the deciding factor.

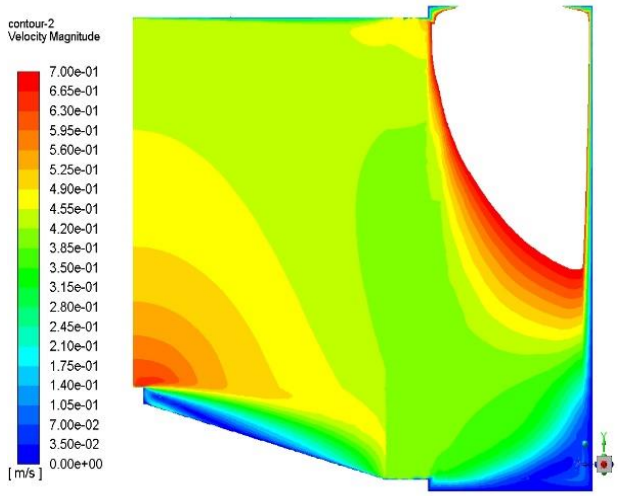

Figure 6-8. Velocity contour of top centre opening (option1)

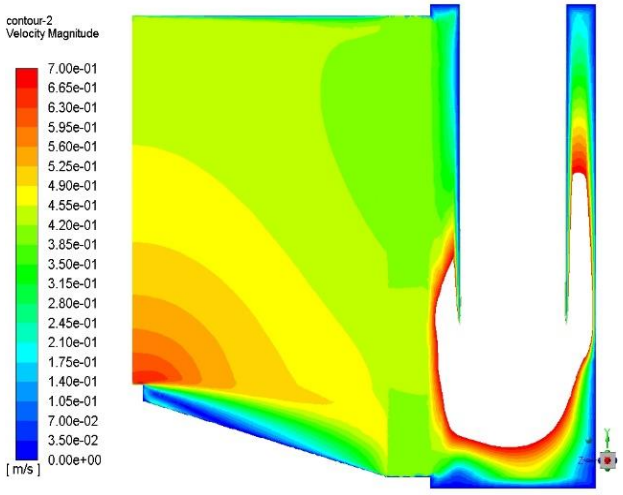

Figure 6-9. Velocity contour of top centre opening with inserted pipe (option 2)

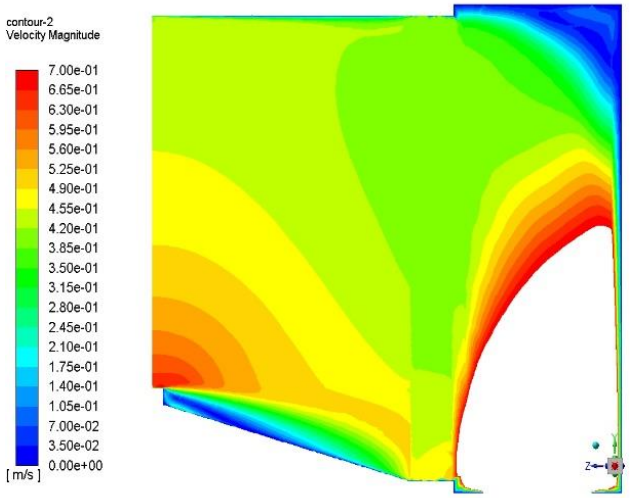

Figure 6-10. Velocity contour of bottom centre opening (option 3)

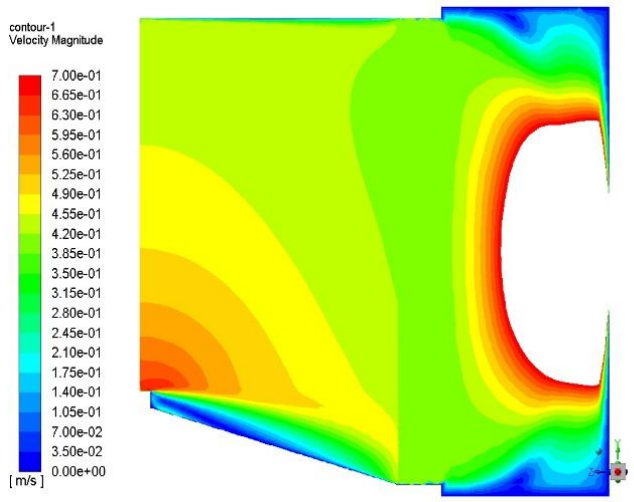

Figure 6-11. Velocity contour of rear opening (option 4)

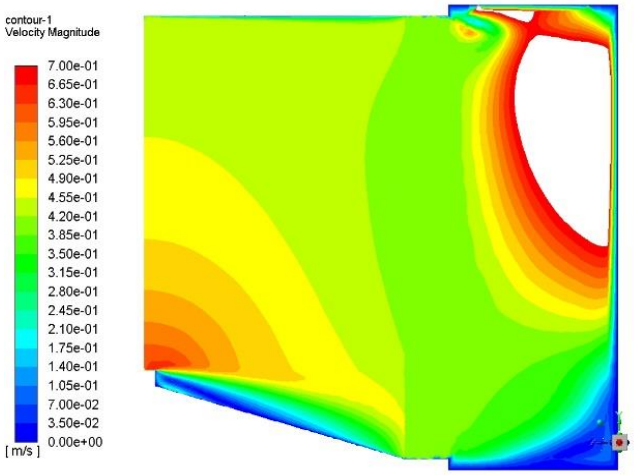

Figure 6-12. Velocity contour of top right and left openings (option 5)

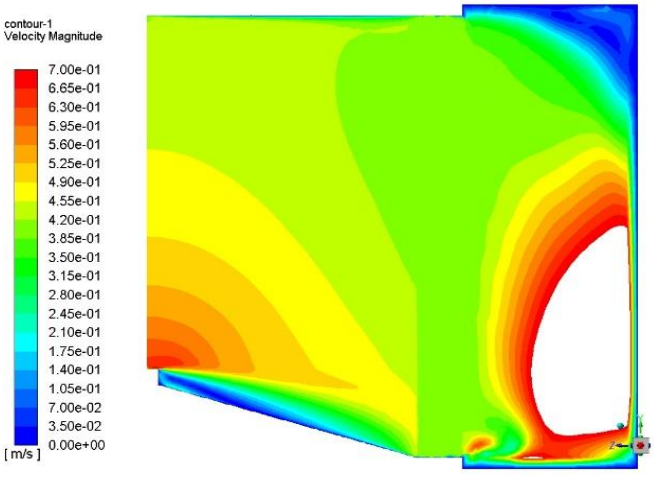

Figure 6-13. Velocity contour of bottom right and left openings (option 6)

6.2 Highest inlet velocity

It is important to have uniform velocity field in the working space i.e., the front box. The uniformity of velocity in the filter vicinity (as discussed in chapter 6.1) is not the deciding criterion as the filter clogging is expected anyway due to the presence of the objects that are to be spray painted. Hence, further simulations for all the six outlet variations as shown in Figure 3-4, were simulated with the highest option for the inlet velocity which is 2.5 m/s to see any changes in the velocity field in the front box which were not seen in the lowest inlet velocity simulations. The following table shows the velocity magnitude for all the outlet options used for the highest inlet velocity.

Table 6-2. Velocity magnitude for outlet variations with the highest inlet velocity

Outlet option	**Inlet velocity [m/s]**	**Inlet surface area [m^2]**	**Inlet volume flow rate [m^3/s]**	**Diameter of the outlet [m]**	**Outlet surface area [m^2]**	**Exhaust velocity [m/s]**
1	2.500	1.140	2.850	0.315	0.0779	36.571
2				0.315	0.0779	36.571
3				0.315	0.0770	36.571
4				0.315	0.0779	36.571
5				2 X 0.225	0.0795	35.839
6				2 X 0.225	0.0795	35.839

The simulations were carried out using velocity inlet with the respective velocity magnitude according to the table 6-2, in the direction normal to the exhaust was taken as exhaust boundary condition. The same standard k-ε model used in the previous set of simulations in the lowest velocity case was used as the turbulent model. After simulating the models the following results were generated.

6.2.1 Velocity vectors

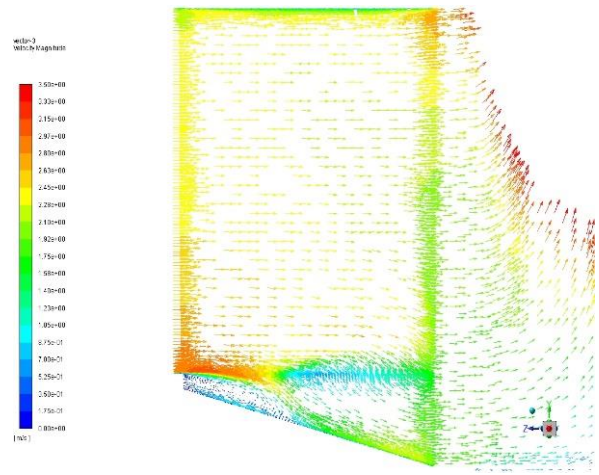

Figure 6-14. Velocity vectors of top centre opening (option 1)

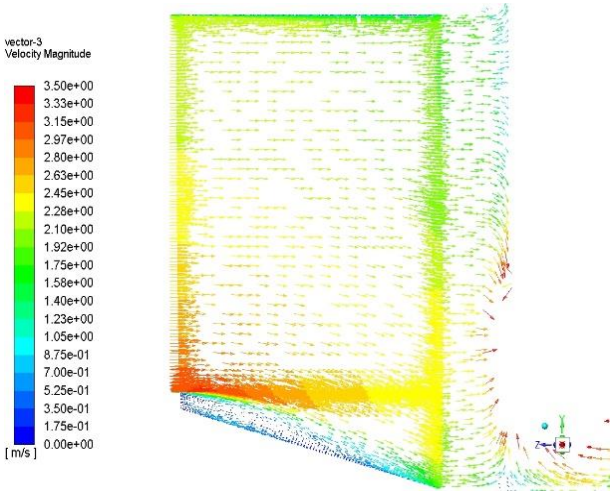

Figure 6-15. Velocity vectors of top centre opening with inserted pipe (option 2)

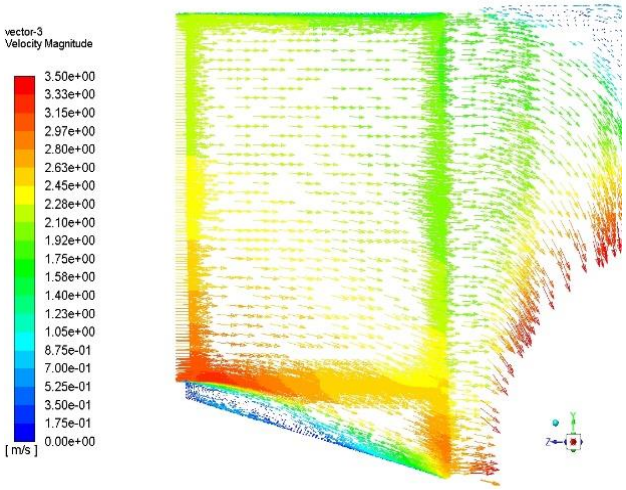

Figure 6-16. Velocity vectors of bottom centre opening (option 3)

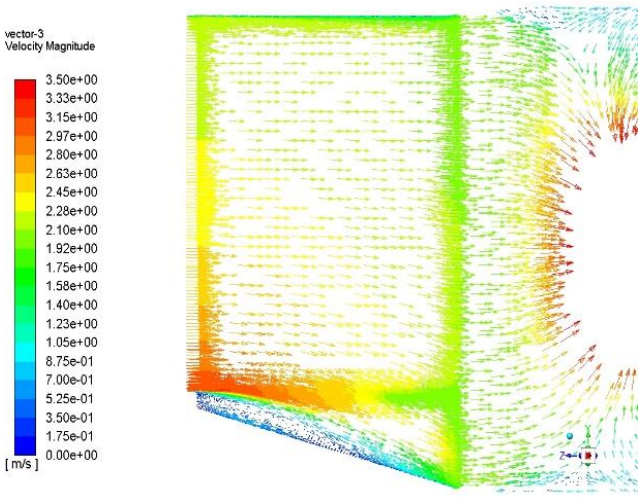

Figure 6-17. Velocity vectors of the rear opening (option 4)

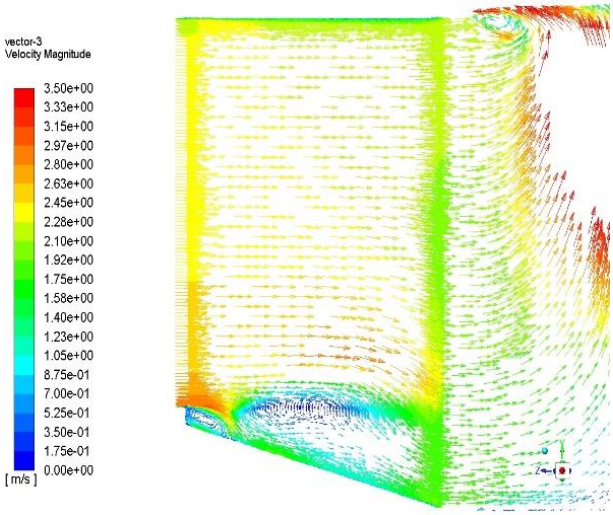

Figure 6-18. Velocity vectors of top right and left openings (option 5)

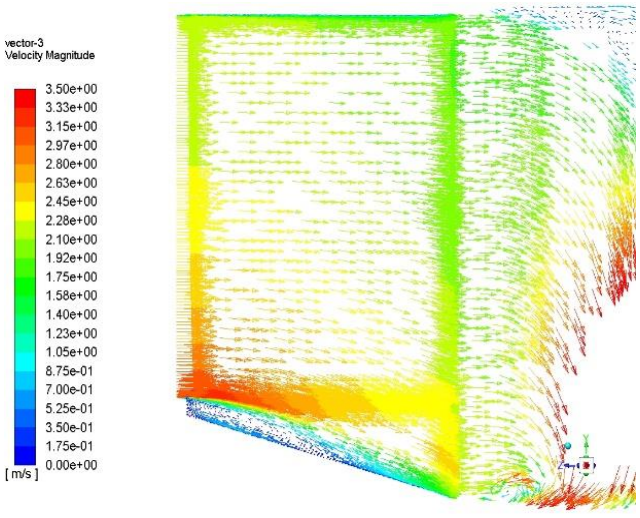

Figure 6-19. Velocity vectors of bottom right and left openings (option 6)

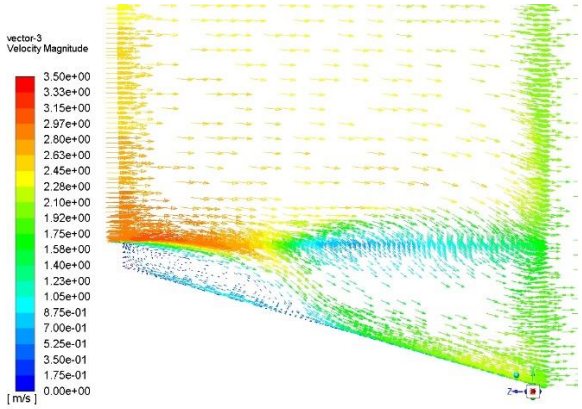

Figure 6-20. Close up of top centre opening

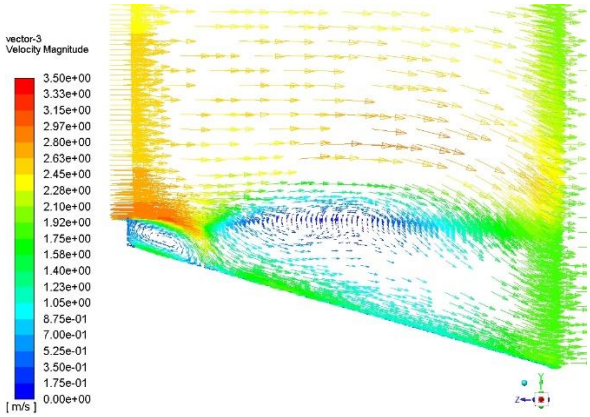

Figure 6-21. Close up of top right and left openings

If the velocity vectors in all the cases are observed, it can be clearly seen that the exhaust outlet options with top centre opening and the top right left openings are the worst as there is a clear non uniformity of velocity field in the region with the perforated plate which can be seen in Figure 6-20 and Figure 6-21. The air returns from the region below the perforated plate into the working space causing a swirl in the centre of the perforated plate, in case of the top right and left exhaust outlets as seen in Figure 6-21. This can cause the paint particles to remain in that region instead of being exhausted which is a big disadvantage. So, these two options are excluded.

In rest of the cases, a similar velocity field can be seen in the working space which makes it hard to decide the best option.

6.2.2 Velocity contours

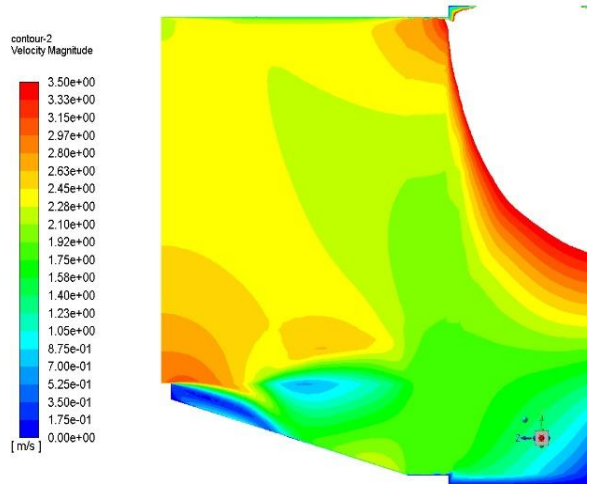

Figure 6-22. Velocity contour of top centre opening (option1)

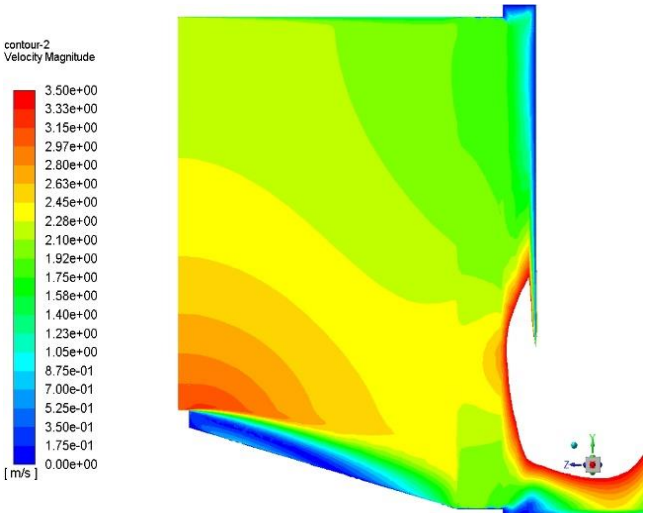

Figure 6-23. Velocity contour of top centre opening with inserted pipe (option 2)

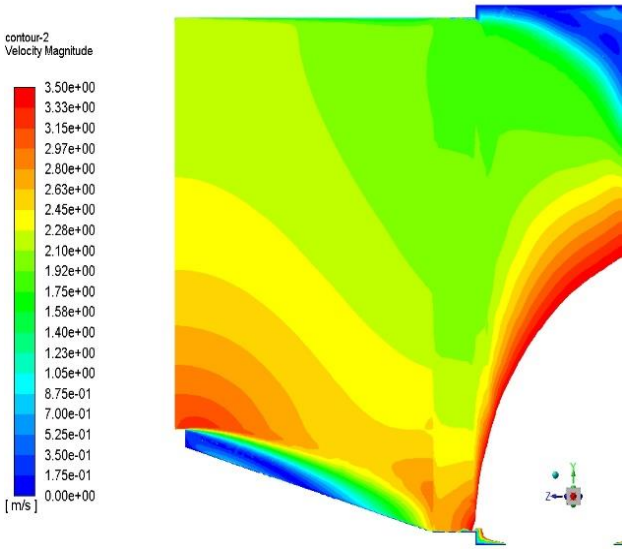

Figure 6-24. Velocity contour of bottom centre opening (option 3)

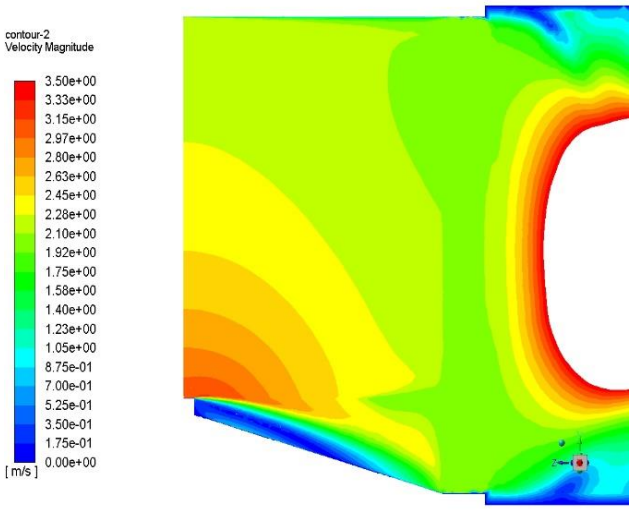

Figure 6-25. Velocity contour of rear opening (option 4)

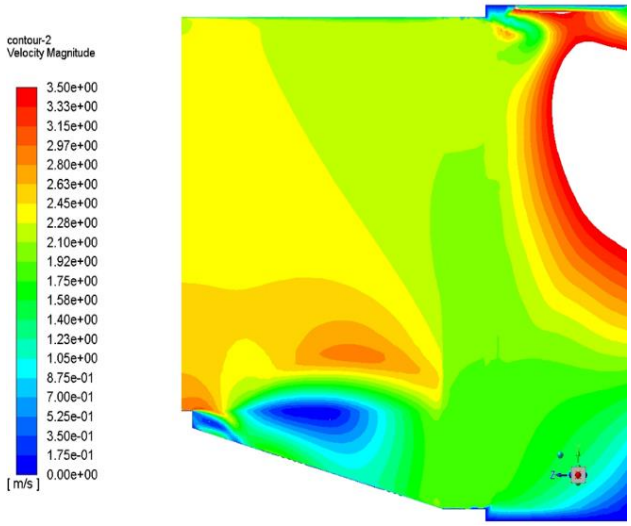

Figure 6-26. Velocity contour of top right and left openings (option 5)

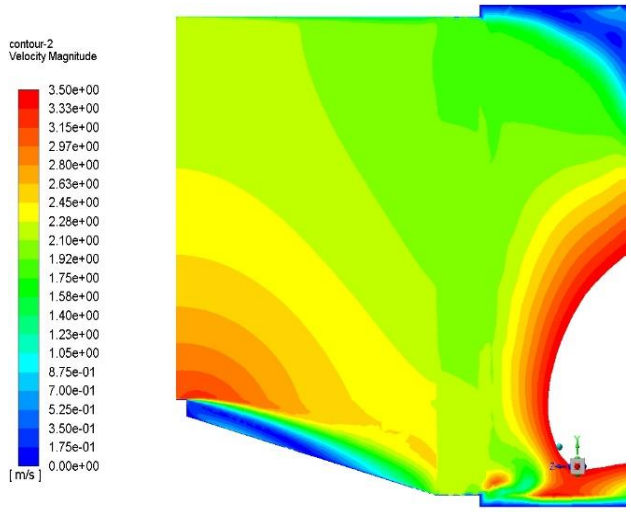

Figure 6-27. Velocity contour of bottom right and left openings (option 6)

Even from the velocity contours, it can be observed that the exhaust options with top centre opening and the top right left openings have a spot in the centre of the perforated plate with a low velocity magnitude. This increases the possibility for the stagnation of paint particles in that region because of not having sufficient exhaust velocity and also because of the swirl and non-uniformity of the velocity field as seen in the velocity vectors, excluding them both for considering as the exhaust outlets.

6.3 Comparison of velocities along the height of the opening in Y-direction

From the previous results, it is quite unclear to finalize on one or two exhaust outlet options. In order to do this, further observations were made by checking all the exhaust outlet options which can provide the minimum inlet velocity i.e., 0.5 m/s in case of lowest inlet velocity and 2.5 m/s in case of the highest inlet velocity along the maximum height of the inlet opening.

The inlet velocities at 0.1 m from the inlet of the working space in x- direction at all the nodes, along its height were exported for all the exhaust outlet option and the following graphs were made using Excel.

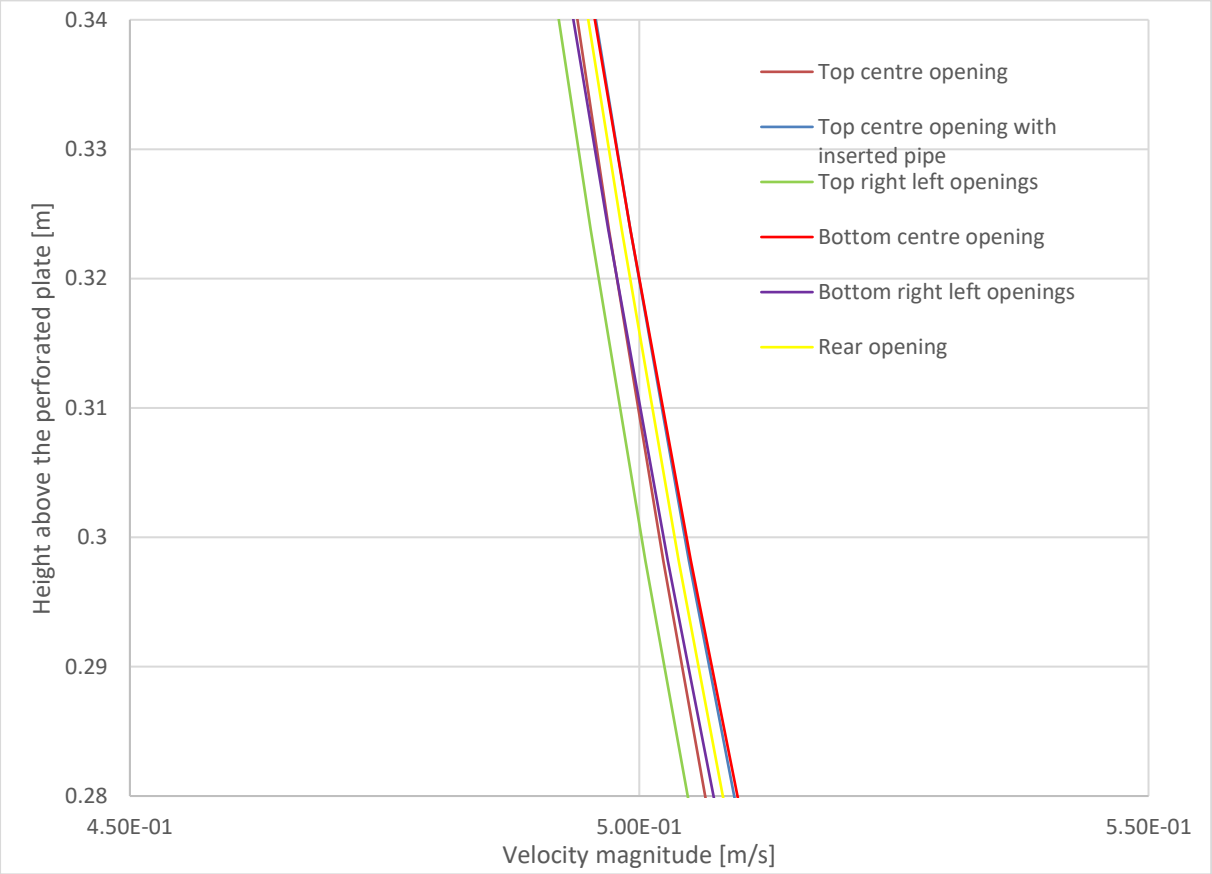

Figure 6-28. Vertical profile of velocity near the inlet for lowest flowrate

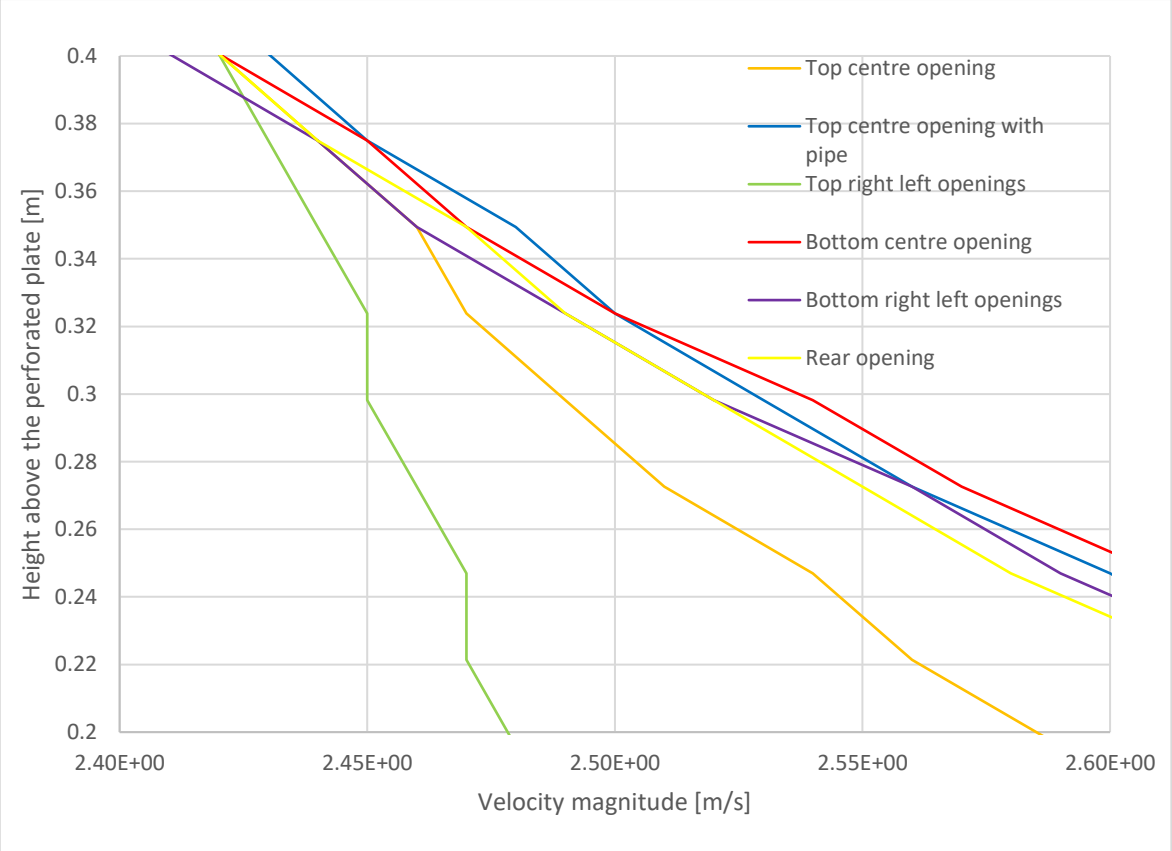

Figure 6-29. Vertical profile of velocity near the inlet for highest flowrate

From both the graphs shown in Figure 6-28 and 6-29, it can be seen that the exhaust outlets with top centre opening with inserted pipe and bottom centre opening provide minimum inlet velocity for both lowest inlet velocity case with 0.5 m/s and the highest inlet velocity case with 2.5 m/s, along the maximum height of the inlet opening compared to the rest of the cases. So, these exhaust options can be finalized as the best options. The option top centre opening with inserted pipe can be selected to save the space in connecting the outlet directly to the exhaust piping without any complications. But, if it is the case that there isn't enough space to connect the outlet to the exhaust piping from the top the bottom centre option can be used.

But, it can be seen in the graphs that in both these exhaust outlet options the maximum height they are able to provide with the minimum inlet velocity is 0.32 m in the lowest inlet velocity case and slightly above 0.32 m in the highest inlet velocity case. The height of the inlet opening is 1 m. So, in both the cases, they are not able to provide the minimum inlet velocity at least for half the height of the opening.

The height of the spray booth from the ground including the pedestal is approximately 2 m. This means that the pedestal is 1 m since the opening is 1 m. If a person who is approximately 1.8m high is working in front of the booth then the most relevant working area will be 1.8 m from the ground.

This means that only 0.8 m of the inlet opening is relevant. This gives the possibility to introduce the inlet option no.2 shown in Figure 3-5, closable opening on the top of the front inlet with dimensions 1140 mm x 330 mm which looks as shown in Figure 6-30. It is predicted that this closable opening can improve the possibility of providing the minimum inlet velocity for the maximum height of the inlet opening since the opening height is reduced.

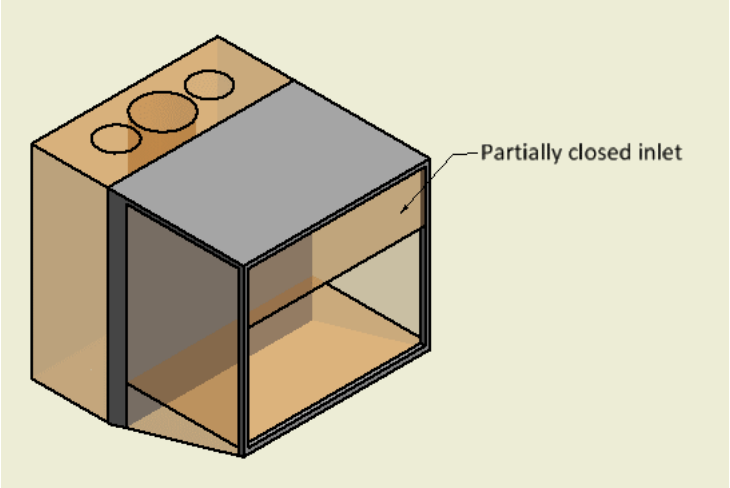

Figure 6-30. Model with partially closed inlet

6.4 Comparison between open inlet and partially closed inlet

Based on the predictions made from the previous results that, partially closing the inlet opening of the working space can improve the possibility of providing the minimum inlet velocity for the maximum height of the inlet opening, the inlet option no.2 was introduced and simulations were carried out.

For both the cases, the lowest inlet velocity and the highest inlet velocity, the exhaust outlet velocities were kept the same as for the cases with completely opened inlets. The cases were simulated with the following results.

Velocity vectors

Lowest inlet velocity

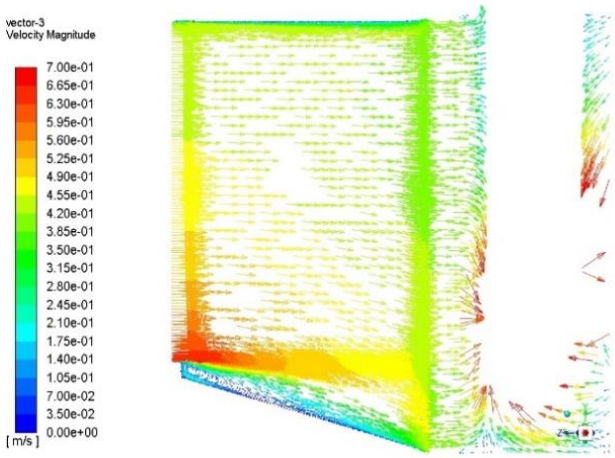

Figure 6-31. Top centre opening with inserted pipe

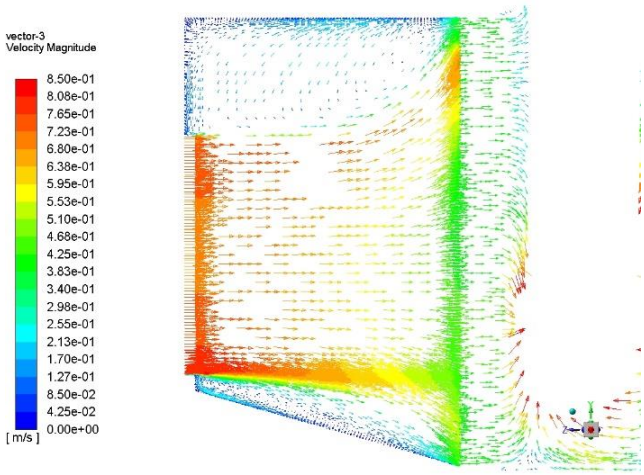

Figure 6-32. Top centre opening with inserted pipe and partially closed inlet

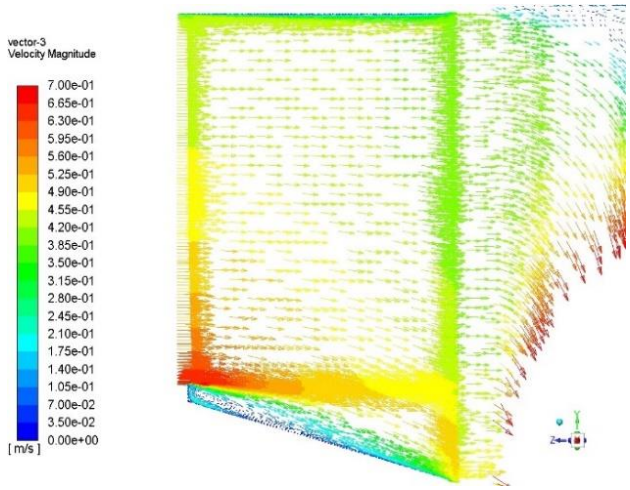

Figure 6-33. Bottom centre opening

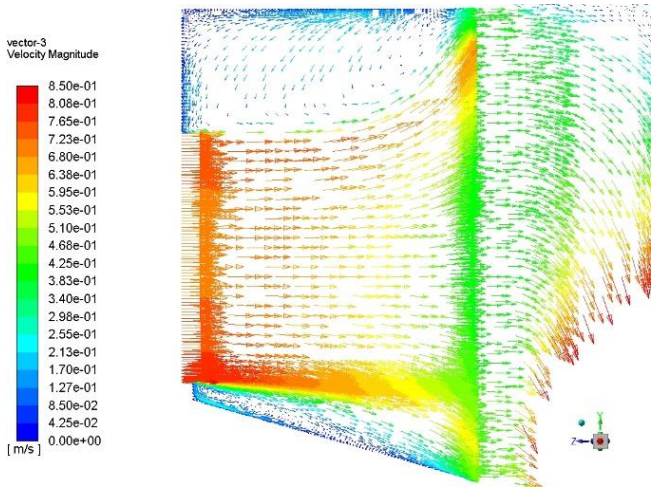

Figure 6-34. Bottom centre opening with partially closed inlet

Highest inlet velocity

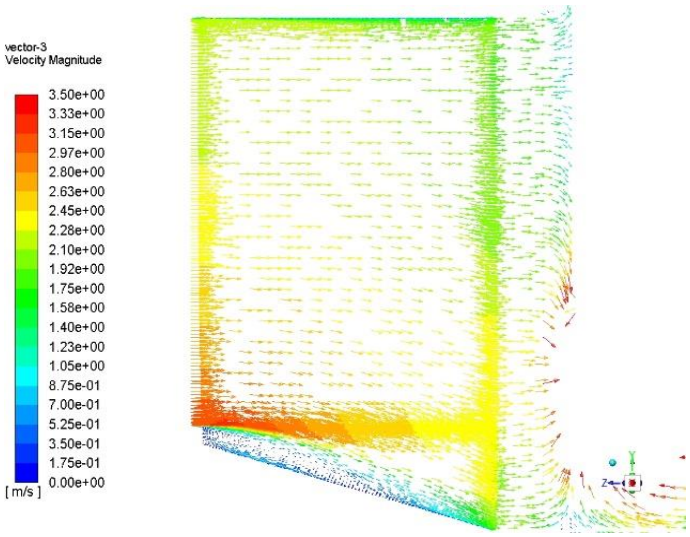

Figure 6-35. Top centre opening with inserted pipe

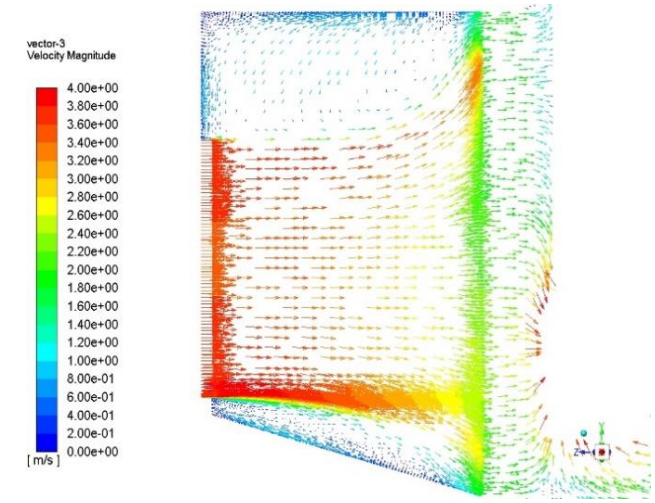

Figure 6-36. Top centre opening with inserted pipe and partially closed inlet

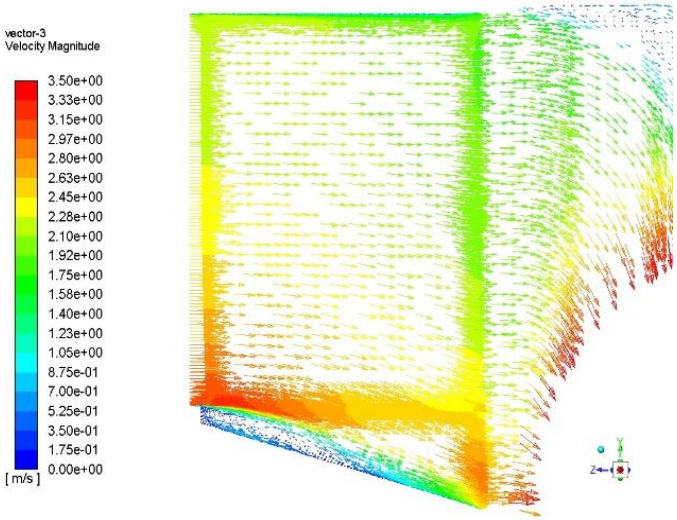

Figure 6-37. Bottom centre opening

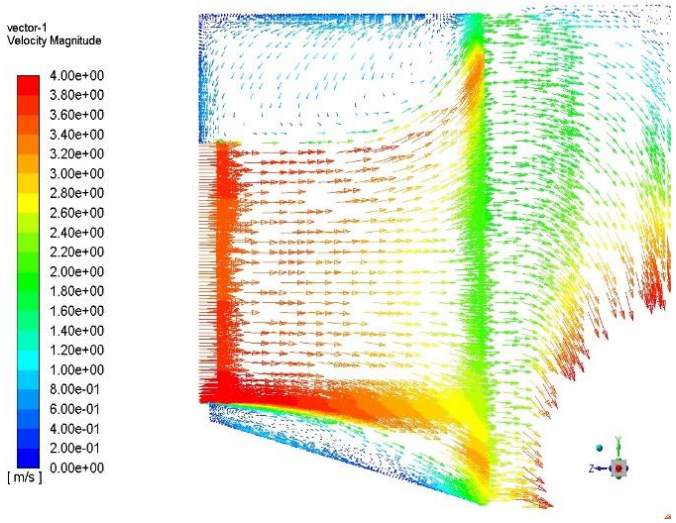

Figure 6-38. Bottom centre opening with partially closed inlet

If the velocity vectors are observed it can be seen in the cases with partially closed inlets that there is definitely an improvement in the velocity magnitude in the inlet. However, a swirl can be seen in the top of the working space for both the outlet options. Due to the steep changes in the inlet and the presence of the corners in the top of the working space the flow is affected forming these swirls. But, the main aim is not to have any paint particles escaping into the ambient space. Also, the paint particles are higher in the lower region of the working space where the high velocity magnitude is necessary to exhaust them, which is possible with the partially closed inlet.

Comparison of velocities along the height of the opening in Y-direction

The inlet velocities at 0.1 m from the inlet of the working space in x- direction at all the nodes, along its height were exported for both the outlet options with and without partially closed inlet in the highest inlet velocity and the lowest inlet velocity cases and the graphs were made using excel.

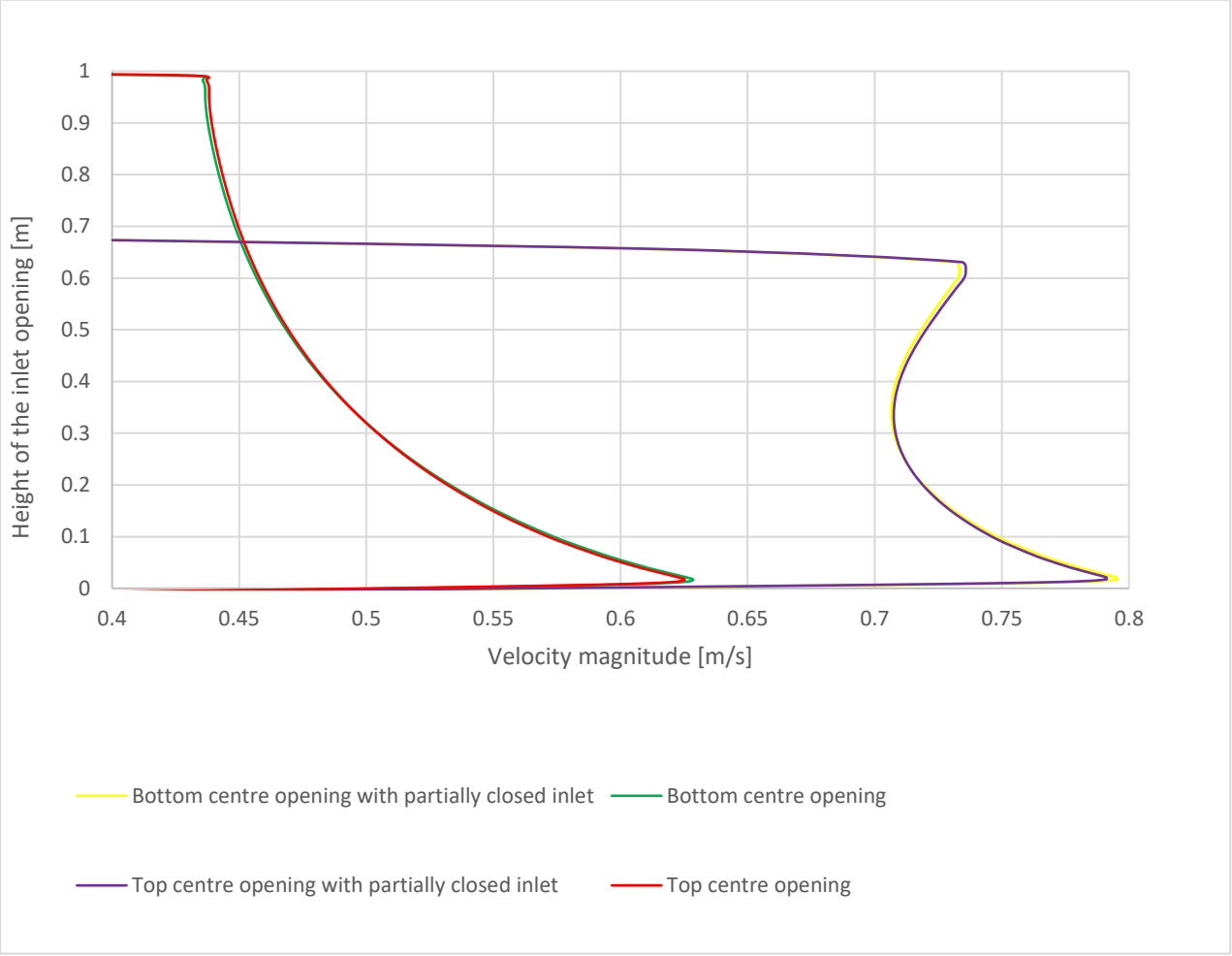

Figure 6-39. Vertical profile of velocity near the inlet for lowest flowrate

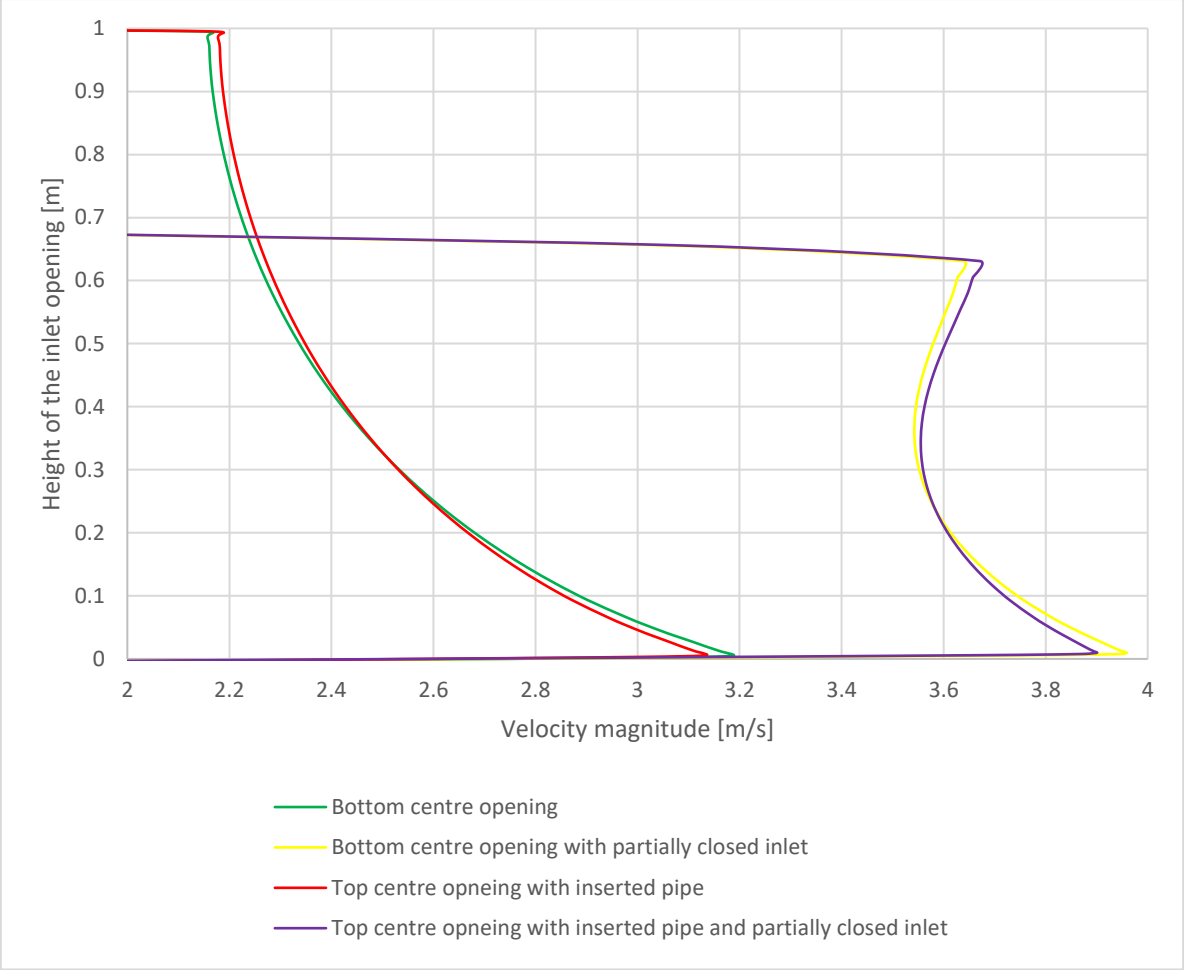

Figure 6-40. Vertical profile of velocity near the inlet for highest flowrate

From the graphs shown in Figure 6-39 and 6-40, it can be seen that the height along the inlet until which the minimum inlet velocity is provided is highest for the cases with partially closed inlet compared to the open inlet. In case of open inlet options, the maximum height is around 0.32m for both the highest and the lowest inlet velocities. Whereas for the partially closed inlet cases it is almost 0.67 m making the relevant working height 1.67 m. This means that relevant working height of 1.8 m of the person is almost covered solving the problem of insufficient velocity magnitude in the working space.

6.5 Particle tracking

In order to track the path of the spray paint particles in the spray booth, a spray paint material was chosen. HAE 30 is a self-priming anti-corrosive water-born paint for steel with density 1230 kg/m^3 (VITON, 2018). An airless sprayer (Control Pro 350 M Airless Paint Sprayer) was chosen with the following parameters (WAGNER, 2018).

Maximum paint flow rate, $\dot{V}_p$ = 2.5 x 10^{-5} m^3/s

Spray pressure, ΔP_s = 110 kPa

Nozzle diameter, d_n = 0.4318 x 10^{-3} m

Maximum spraying velocity, u_s = 170.72 m/s

According to Hinds, the spray paint particle diameter ranges from 2 to 1000 µm (Hinds, 1999), which is a huge range. But the spray paint particles usually range from 30 to 50 µm (Brosseau et al., 1992). So, based on these sources of information, two particles sizes, 5 and 50 µm were selected to track.

6.5.1 Discrete phase model

The tracking of the spray paint particles in the spray booth was done using the Discrete Phase Model (DPM) in ANSYS Fluent. The uncoupled DPM was used, so the particles do not influence the fluid flow.

Physical models enabled for the DPM are

1. Drag Force
2. Saffman Lift Force
3. Virtual Mass Force

Initial Conditions for the Discrete Phase

The particle injection was made using a solid cone injection. Following are the inputs.

Point properties

1. Position: The coordinates of the origin of the spray cone in the X, Y, and Z position fields were given so that it lies in the centre of the front inlet of the model.
2. Diameter of the particles: 5 and 50 µm.
3. Azimuthal start angle: 0^o

4. Azimuthal stop angle: 360^{o}
5. Axis: The direction of the spray was defined using X,Y, and Z axis fields, which is Z axis for the model.
6. Velocity magnitude: The spraying velocity take was half of the maximum spraying velocity, 85 m/s.
7. Cone angle: 90^{o}
8. Outer radius: 0.1 m
9. Mass flow rate: 0.0153 kg/s
10. Particle type: inert

Turbulent dispersion

Stochastic tracking with discrete random walk model and random eddy lifetime were selected.

No. of tries used: 5

With all the above inputs the particle tracking was made for the two selected options of exhaust outlets with and without the partially closed inlet.

6.5.2 Comparison of particle tracking between open inlet and partially closed inlet

Particle tracking is relevant only in the working section as the PorZo tool used to define the filter media just mimics the pressure loss caused by the filter. It does not act like an actual filter to capture the paint particles. In all the following figures it can be seen that none of the paint particles are trapped in the filter region. They just pass through the filter. So, the behaviour of the particles in the working section can only be considered.

Particles of 5µm diameter

Firstly the particles with diameter of 5 µm were tracked with the following results.

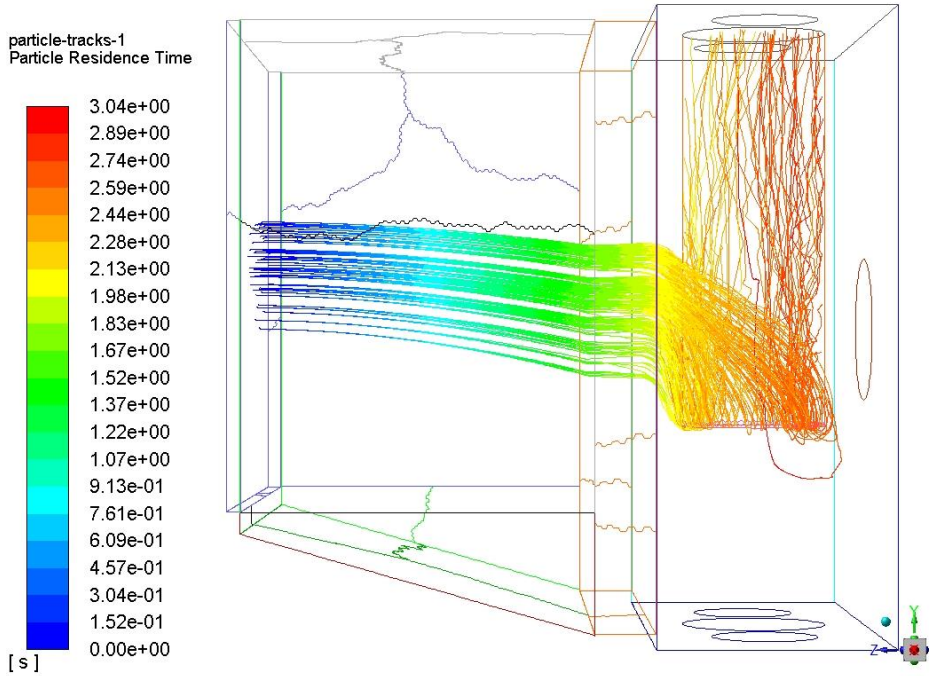

Figure 6-41. Top centre opening with inserted pipe and open inlet

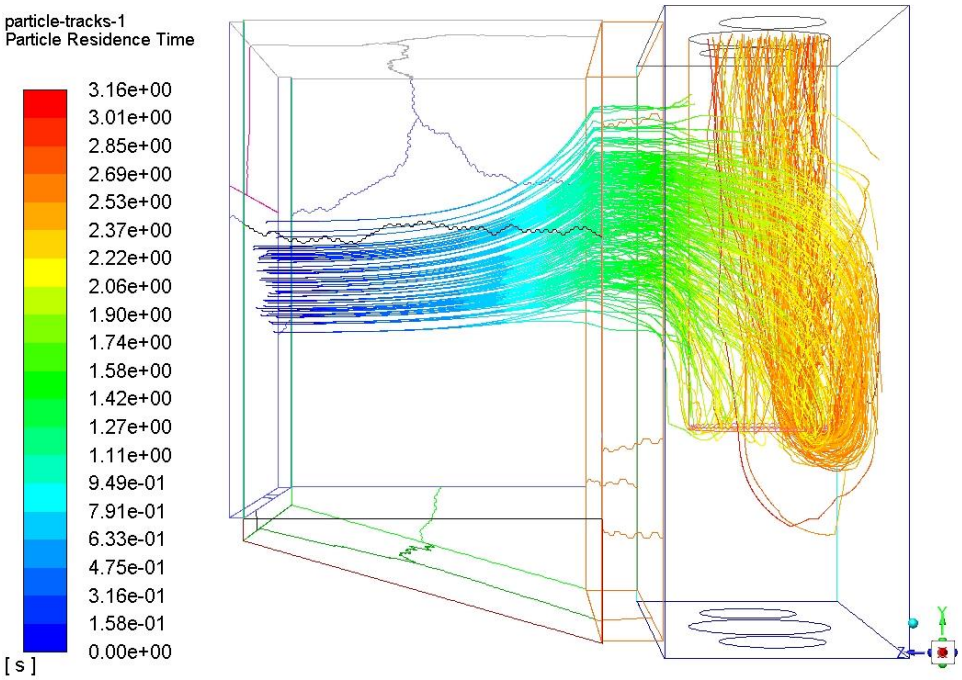

Figure 6-42. Top centre opening with inserted pipe and partially closed inlet

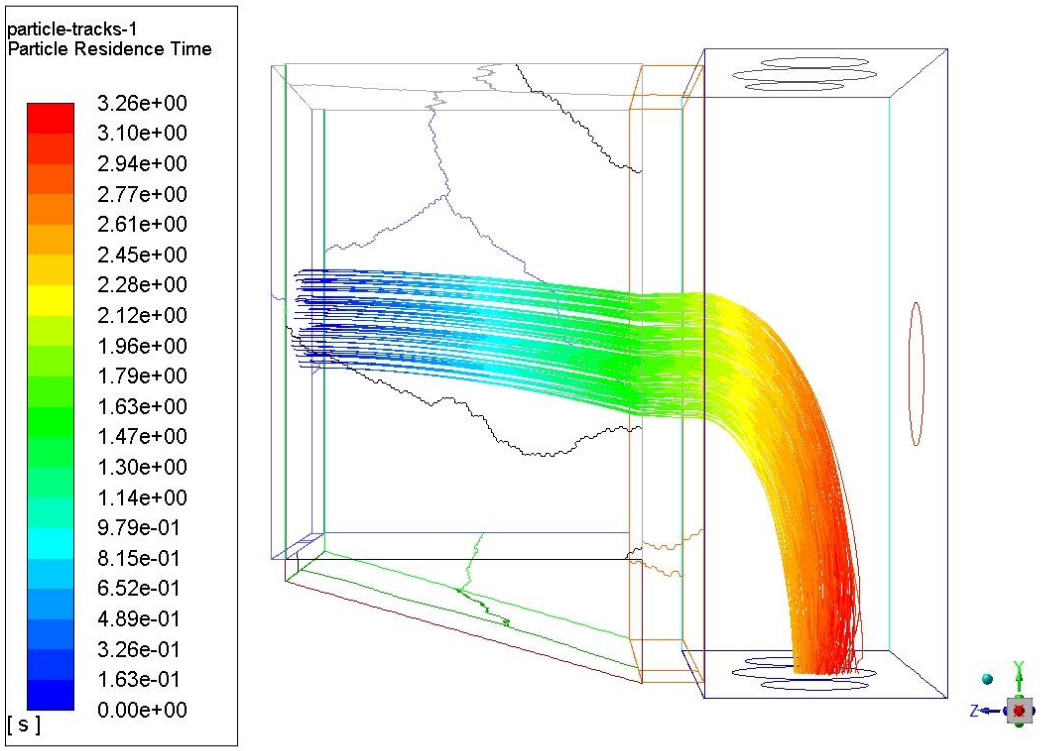

Figure 6-43. Bottom centre opening with open inlet

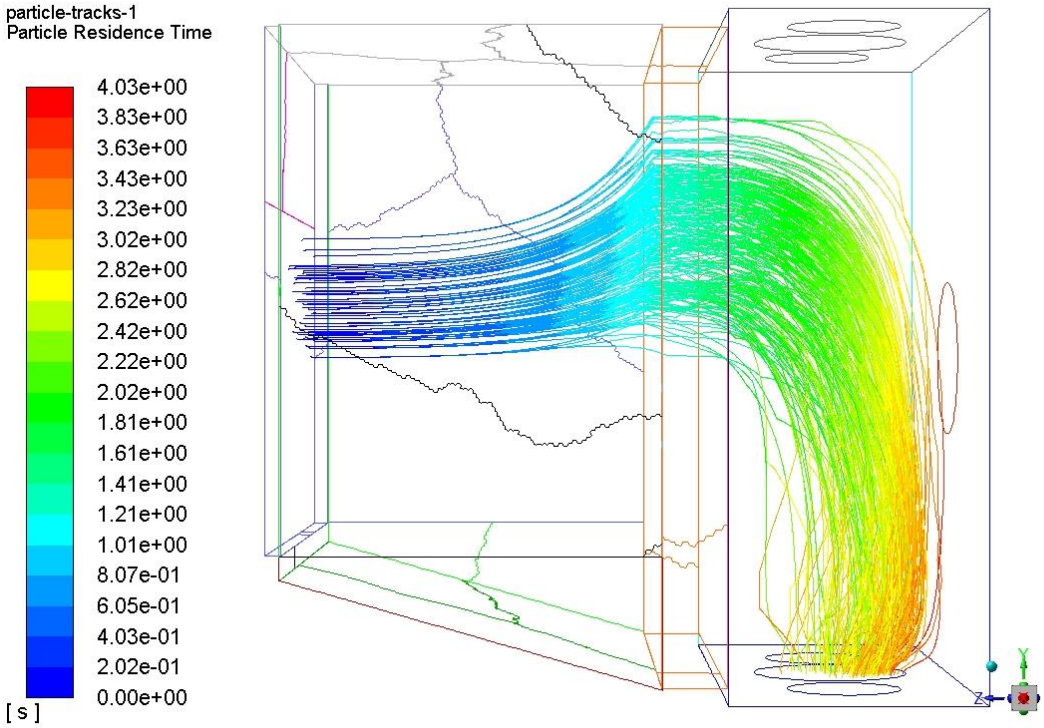

Figure 6-44. Bottom centre opening with partially closed inlet

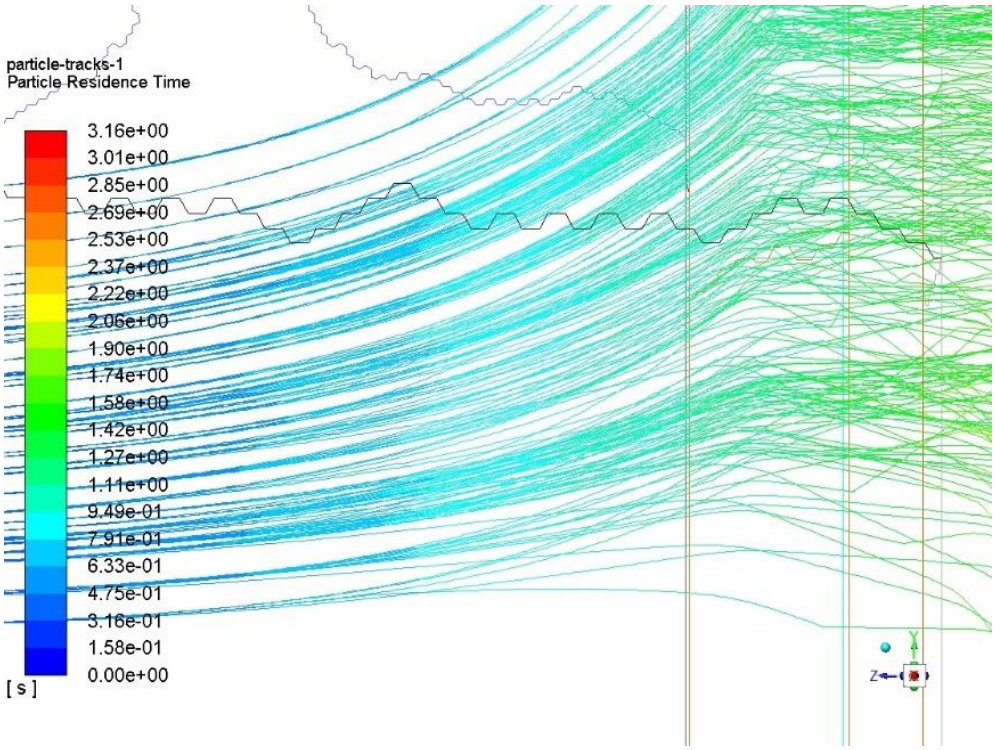

Figure 6-45. Close up of the particle streams

It can be observed in the Figures 6-41, 6-42, 6-43 and 6-44 that the residence time of the particle in the cases with open inlet is slightly more than that of the cases with partially closed inlet. Due to the higher velocity magnitude in the working space for the partially closed inlets this can be seen. Since the size of the particle is quite low, the inertia is low too and any deviation of the particles from the air flow in the working space cannot be seen. All the particles seem to follow the air flow. It can also be seen that the flow is almost laminar for most of the depth of the working space and when the flow approaches the filter it is converting into turbulent as seen is Figure 6-45.

Particles of 50µm diameter

In order to observe the difference in the particles with larger diameter, particles of 50 µm were tracked with the following results.

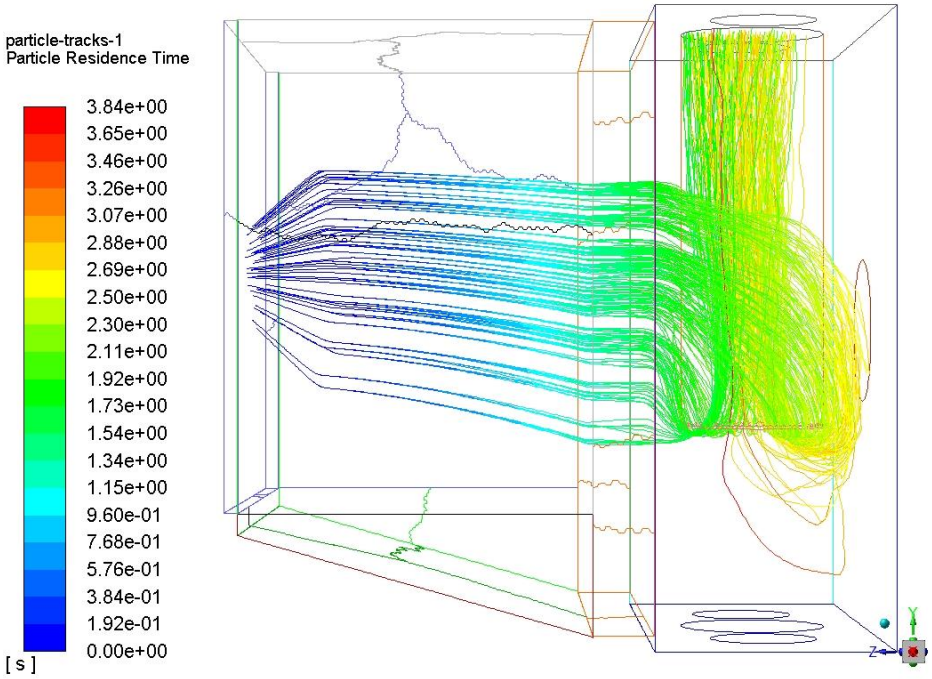

Figure 6-46. Top centre opening with inserted pipe and open inlet

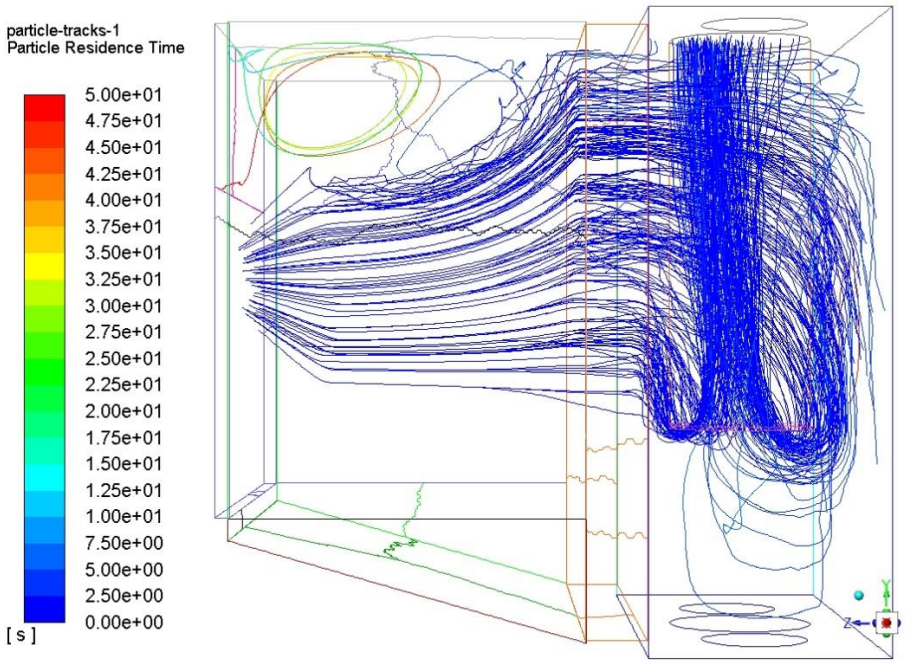

Figure 6-47. Top centre opening with inserted pipe and partially closed inlet

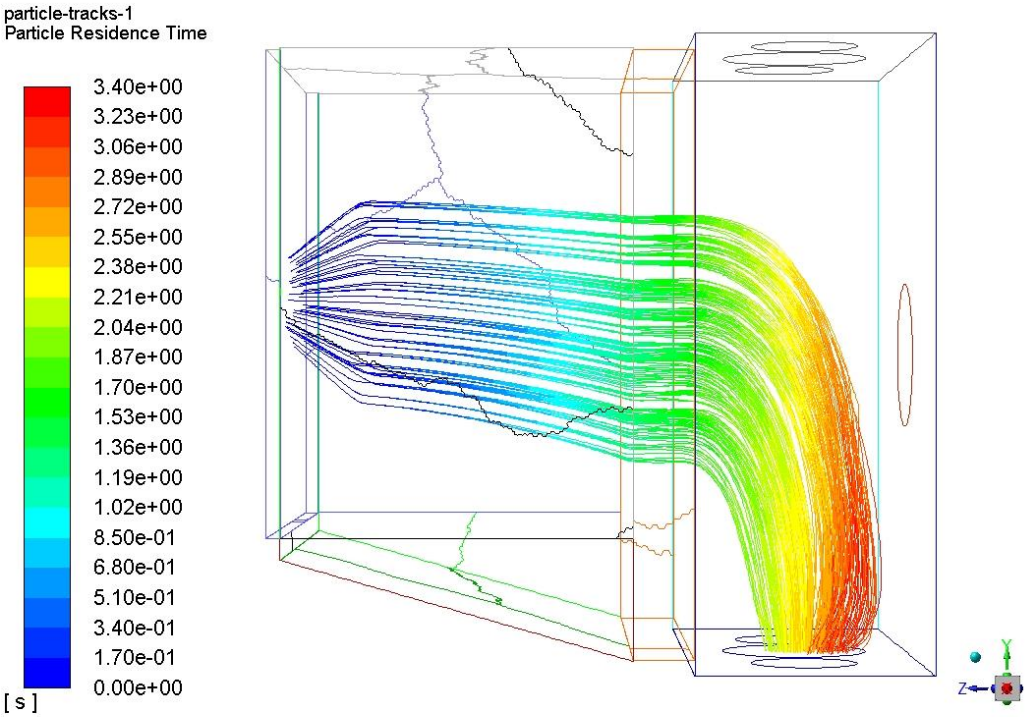

Figure 6-48. Bottom centre opening with open inlet

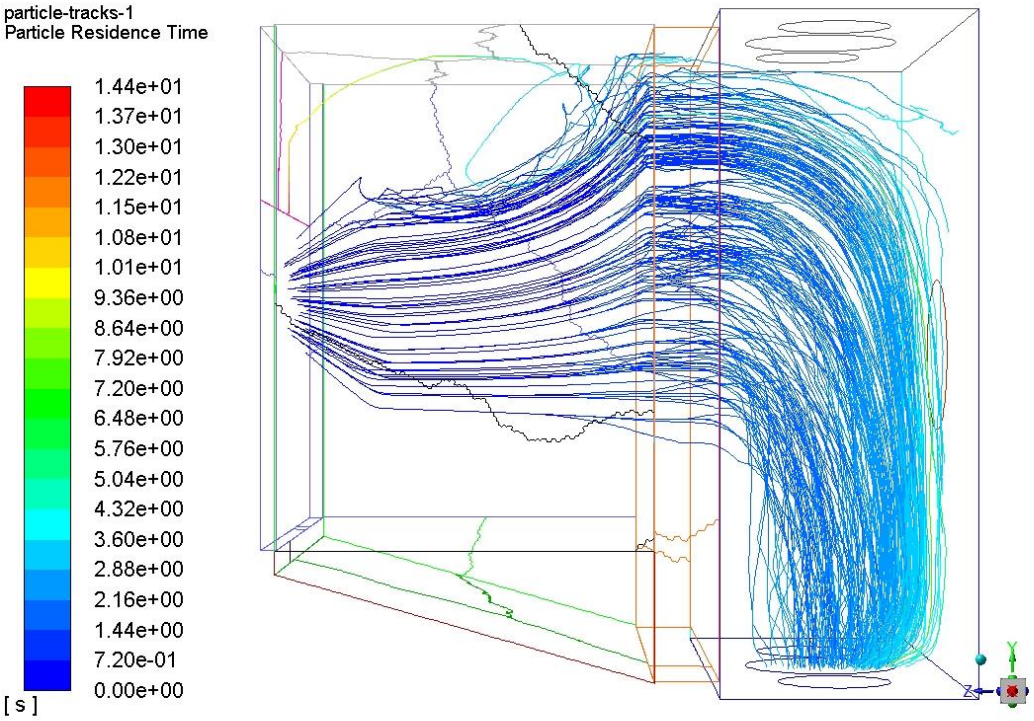

Figure 6-49. Bottom centre opening with partially closed inlet

If the Figure 6-50, is observed it can be seen that the almost laminar flow changes to turbulent flow as seen in case of the smaller particles as the particles approach the filter in Figure 6-45.

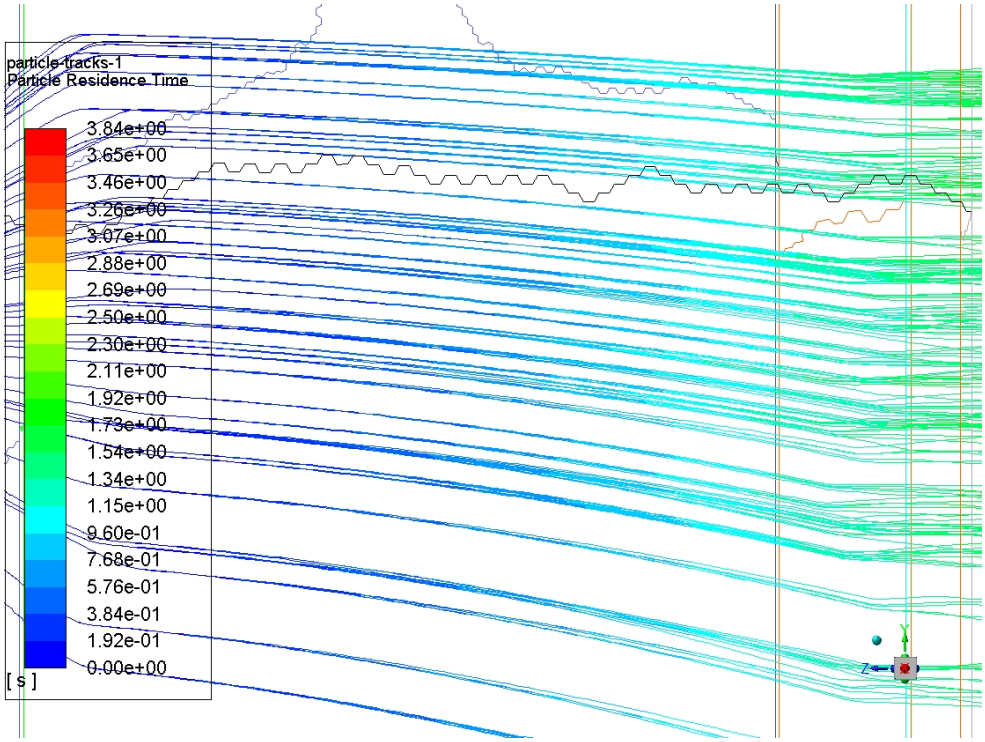

Figure 6-50. Close up of particle streams

If Figures 6-46, 6-47, 6-48 and 6-49 are observed it can be clearly seen that the particle size makes a difference in the path of the particles at the initial stage. Due to the inertia of the particles, they travel in the path of the cone at the beginning of the flow and later follow the air flow.

But, if a comparison was made between the partially closed inlet and the open inlet, it can be seen that the flow is much uniform in case of the open inlet. The particles in the partially closed cases seem to follow the swirl motion of the air in the top corners. This is undesirable because this can cause the paint particles to stain the walls of the booth and also disturb the spray pattern causing an unnecessary over spray.

Although the cases with open inlet have a higher particle residence time, they seem to have a much more uniform flow. A desirable and almost laminar flow for the most part of the working space can be achieved. This particle tracking shows that the partially closed inlet can be used in the case of small paint particles. Whereas in case of larger particles the open inlet functions better. But, in all the cases we can see that none of the particles are escaping into the environment through the booth inlet.

7. Conclusion

The aim of the thesis was to study the exhaust outlet and inlet variants of a portable spray booth by the analysis of fluid flow in the working space and particle transfer to the filtration system based on CFD simulations. It was decided to study six exhaust outlet options and two inlet options. Every variant was studied for two inlet velocities, 0.5 m/s which is the lowest case and 2.5 m/s, the highest case. ANSYS Fluent with the standard K-epsilon (k-ε) turbulence model and velocity outlet was used for the simulation of all the variants. For all the variants the velocity vectors and velocity contours were studied to see the differences.

In the initial stage, the results for the low velocity cases did not have any significant differences in the velocity vectors in the working space for all the variants. So, all the exhaust outlet variants were simulated with the highest inlet velocity to see any changes in the velocity field in the front box which were not seen in the lowest velocity simulations. After observing the velocity vectors and the velocity contours in all the cases it was obvious that the exhaust outlet option with the top centre opening and the option with top right & left openings were the worst of all and were excluded from the study.

Out of all the exhaust outlet options, the one that can provide the required minimum inlet velocity for both lowest inlet velocity and the highest inlet velocity, along the maximum height of the inlet opening was checked. It was seen that the exhaust outlet option with top centre opening with inserted pipe and the option with the bottom centre opening provided the required minimum inlet velocity for the maximum height of the booth inlet opening. So, these two exhaust outlet options were finalised. Introducing a partially closed inlet in the top of the front opening significantly improved the ability to provide a minimum inlet velocity for the open part of the booth front opening.

Paint particles with two size variants were tracked for both the outlets options with and without the partially closed inlet using the discrete phase model. It was seen that in case of small particles all the variants worked well. But, for larger particles due to the inertia of the particles, some of them were not exhausted but remained in the working space for the options with partially closed inlet. This gave the conclusion that for particles with larger sizes the partially closed inlet variants are not the best options.

Finally it was concluded that exhaust outlet options with top centre opening with inserted pipe and bottom centre opening are the best ways to exhaust the paint particles providing a desirable, almost laminar flow in the working space. The usage of the partially closed inlet can be used when the particles are smaller to provide better velocity magnitude in the working space.

In this study, several aspects were simplified to reduce the complexity of the problem and respect the time constraint. The filter media and the perforated plate were defined using the PorZo tool which does not create an actual filter media but just creates a pressure loss caused by the presence of the filter. This gives the disadvantage of not being able to check the filter efficiency. The ambient environment around the spray booth was not included which may give even realistic results. The particles were also considered as inert and not changing due to evaporation. The discrete phase model was uncoupled i.e., without the influence of the particles on the air flow. No objects were placed in the working space and no person was placed in front of the spray booth which would have caused turbulence. For further investigation, all these aspects can be improved to obtain more realistic results.

8. Bibliography

ANSYS. (2018). Ansys 19 Documentation. Ansys, Inc.

Bakker, A. (2018). *The Colorful Fluid Mixing Gallery.* Retrieved from bakker.org: http://www.bakker.org/dartmouth06/engs150/15-dpm.pdf (Available on 20 June 2018)

Brosseau, L. M., Fang, C. P., Snyder, C., & Cohen, B. (1992). Particle Size Distribution of Automobile Paint Sprays. *Applied Occupational and Environmental Hygiene*, Pages 607-612.

Chang, N. K., Woo, H. C., Suk, J. C., Chang, H. P., & Dong, S. K. (2002). Elsevier Science Ltd.

CJ Coatings UK. (2018). Retrieved from cjcoatings.co.uk: https://www.cjcoatings.co.uk/2016/07/what-is-spray-painting (Available on 20 June 2018)

Hejma, J., Budinsky, K., Vavra, A., & Drkal, F. (1981). *Vzduchotechnika v drevozpracovavajicim prumyslu.* Praha: SNTL.

Hinds, W. C. (1999). *Aerosol Technology.* Toronto: John Wiley & Sons. Inc.

Jicolor, s.r.o. (2018). Retrieved from www.lakyrmat.cz: http://www.lakyrmat.cz/www-lakyrmat-cz/eshop/8-1-Strikaci-pistole-a-lesticky/-4-/5/331-Strikaci-pistole-Delta-DL-1000MP-1-8mm (Available on 20 June 2018)

KS Klima Service. (2014). Air Filters and Filtration Equipment(Catalogue). Dobris.

Launder, B. E., & Spalding, D. B. (1972). *Lectures in Mathematical Models of Turbulence.* London, England: Academic Press.

pati. (2018). Retrieved from pati.org: http://www.pati.org/Journey%20Test%20Study%20Guide/Spray%20Painting.pdf (Available on 20 June 2018)

Ron Joseph & Associates. (1991). *RJA. Spray Booth Design and Maintenance for Pollution Prevention.* Ron Joseph & Associates, Inc.

Talbert, R. (2008). *Paint Technology Handbook. Chapter 8-Spray Booths.* CRC Press(Taylor & Francis Group).

VITON, s.r.o. (2018). Retrieved from barvy-viton.cz: https://www.barvy-viton.cz/en/search/?f_Act=Search&f_hledane=HAE+30&f_ActSubmit= (Available on 20 June 2018)

Vondál, J. (2018, January 9). *SVSFEM.* Retrieved from svsfem.cz: https://www.svsfem.cz/produkty/aplikace-ansys-act/porzo#download (Available on 09 January 2018)

WAGNER, GmBH. (2018). Retrieved from wagner-group: https://www.wagner-group.com/uk/consumer/product/control-pro-350-m-airless-paint-sprayer/ (Available on 20 June 2018)

White, F. M. (1999). In F. M. White, *Fluid Mechanics* (Fourth ed., pp. 438, 442). WCB McGraw Hill.

Zelenský, P., & Švandová , K. (2018). *Návrh průmyslového lakovacího boxu pro protypové studium [Technical report].* Kladno: PŽS - Engineering s.r.o.